Copy 5
RM L52C25

NACA RM L52C25

NACA

RESEARCH MEMORANDUM

EFFECTS OF CHORD DISCONTINUITIES AND CHORDWISE FENCES ON LOW-SPEED STATIC LONGITUDINAL STABILITY OF AN AIRPLANE MODEL HAVING A 35° SWEPTBACK WING

By Byron M. Jaquet

Langley Aeronautical Laboratory
Langley Field, Va.

NATIONAL ADVISORY COMMITTEE
FOR AERONAUTICS

WASHINGTON
June 24, 1952

NATIONAL ADVISORY COMMITTEE FOR AERONAUTICS

RESEARCH MEMORANDUM

EFFECTS OF CHORD DISCONTINUITIES AND CHORDWISE FENCES ON LOW-SPEED STATIC LONGITUDINAL STABILITY OF AN AIRPLANE MODEL HAVING A 35° SWEPTBACK WING

By Byron M. Jaquet

SUMMARY

A low-speed investigation was made in the 6- by 6-foot test section of the Langley stability tunnel to determine the effects of chord discontinuities and chordwise fences on the static longitudinal stability and wake characteristics of an airplane model having a 35° sweptback wing.

The use of a fence or a 10-percent-semispan chord-extension, with the inboard face of the chord-extension at the same spanwise location as the fence, caused a slight improvement in the static longitudinal stability of the basic wing alone at moderate angles of attack which resulted from an improvement in the flow over the tip of the wing and higher tip loadings for a given angle of attack.

A fence located at 68-percent semispan from the plane of symmetry or a 10-percent-semispan chord-extension with the inboard face at the same spanwise location as the fence reduced the instability of the plain complete model at moderate angles of attack to neutral stability. The fence acted as a physical barrier to the leading-edge separation vortex thereby improving the flow over the wing outboard of the fence. The main effect of the fence was to provide a more favorable variation of downwash angle with angle of attack at the horizontal tail. The chord-extension provided an aerodynamic barrier in addition to a physical barrier to the separation vortex. The aerodynamic barrier was a vortex along the inboard face of the chord-extension. The chord-extension also mainly provided a more favorable variation of downwash angle with angle of attack at the horizontal tail. The chord recessions investigated did not appreciably reduce the instability of the plain complete model because of a lack of an aerodynamic or physical barrier to the separation vortex.

INTRODUCTION

A low-speed investigation of an airplane model having a 35° sweptback wing has indicated that the instability which occurred at low angles of attack and was attributable to an unstable variation of downwash angle with angle of attack at the horizontal tail could be eliminated by the use of a chordwise fence (reference 1) or by lowering the horizontal tail to the fuselage center line (reference 2). Only neutral stability was obtained by either method, however. The effects of the fence (reference 1) on the longitudinal stability of the model varied considerably with spanwise position of the fence.

Two low-speed investigations, one of a 60° sweptback wing (reference 3) and one of two 52° sweptback wings (reference 4), have indicated that a marked improvement in the static longitudinal stability of a wing alone can be obtained with the use of small chord-extensions with results similar to those which would be expected with a chordwise fence. The investigation of reference 1 did not determine the effects of the fence on the flow over the wing surface or in the wing wake. Visual observations of the effects of chord-extensions on the flow over the wings were made in the investigations reported in references 3 and 4, however.

The present investigation was made to determine the effects of various chord discontinuities and chordwise fences on the static longitudinal stability characteristics of an airplane model having a 35° sweptback wing. In addition, downwash, sidewash, and dynamic-pressure measurements were made with various chord discontinuities mounted on the model. These surveys were made in the plane of the horizontal tail along a line passing through the tail aerodynamic center.

SYMBOLS

The data presented herein are in the form of standard NACA symbols and coefficients of forces and moments and are referred to the stability system of axes with the origin at the projection of the quarter-chord point of the mean aerodynamic chord on the plane of symmetry. The positive direction of the forces, moments, and angular displacements is shown in figure 1. The coefficients and symbols used herein are defined as follows:

C_L lift coefficient $\left(\frac{L}{qS_w}\right)$

$C_{L_{max}}$ maximum lift coefficient

C_D	drag coefficient $\left(\frac{D}{qS_w}\right)$
C_m	pitching-moment coefficient $\left(\frac{M}{qS_w\bar{c}_w}\right)$
L	lift, pounds
D	drag, pounds
M	pitching moment, foot-pounds
A	aspect ratio $\left(b^2/S\right)$
b	span, feet
S	area, square feet
c	local chord parallel to plane of symmetry, feet
$\bar{c}$	mean aerodynamic chord, feet $\left(\frac{2}{S}\int_0^{b/2} c^2 dy\right)$
ρ	density of air, slugs per cubic foot
V	free-stream velocity, feet per second
$\frac{q_t}{q}$	measured ratio of dynamic pressure at horizontal to free-stream dynamic pressure
q	free-stream dynamic pressure, pounds per square foot $\left(\frac{1}{2}\rho V^2\right)$
q_t	dynamic pressure at horizontal tail, pounds per square foot
ϵ	measured downwash angle, degrees
σ	measured sidewash angle (positive when it tends to decrease angle of attack of vertical tail), degrees
i_w	incidence of wing-root-chord plane with respect to fuselage center line, degrees (3° for model of this investigation)
α	angle of attack of fuselage center line, degrees (angle of attack of wing is related to angle of attack of fuselage center line by $\alpha_w = \alpha_F + i_w$ (see fig. 1))

[redacted]

y spanwise distance measured perpendicular to plane of symmetry, feet

$C_{L_\alpha} = \frac{\partial C_L}{\partial \alpha}$

$C_{m_{C_L}} = \frac{\partial C_m}{\partial C_L}$

Subscripts:

F fuselage

H horizontal tail

w wing

For convenience, the following notation will be used to denote the various model components:

W wing

W + F + V wing, fuselage, and vertical tail

W + F + V + H wing, fuselage, vertical and horizontal tails

APPARATUS, MODEL, AND TESTS

The present investigation was conducted in the 6- by 6-foot test section of the Langley stability tunnel with the model mounted at the origin of the axes system (projection of quarter-chord point of the mean aerodynamic chord on plane of symmetry) on a single support strut. The strut was attached to a six-component balance system.

The fuselage and the vertical and horizontal (0° incidence) tails were previously used for the investigation reported in reference 2. The basic wing was the same as that used for the investigation of reference 2 and had a removable leading-edge section extending from $0.68\frac{b_w}{2}$ to the wing tip to enable various chord discontinuities to be used interchangeably. The basic wing had the 0.333 chord line swept back 35°, an aspect ratio of 3.57, a taper ratio of 0.565, an area of 2.975 square feet, and a mean aerodynamic chord of 0.942 foot. Details of the basic model are shown in figure 2. Additional details of the basic model can be obtained

from reference 2. The various chord discontinuities and chordwise fences used in the investigation are shown in figure 3. The chord-extensions and chord-recessions were formed by extending or recessing the wing leading edge by $0.10\bar{c}$. Photographs of some model configurations and the wake-survey apparatus used in this investigation are presented as figure 4. The wake-survey apparatus consisted of a yaw-head pitot tube mounted on a frame attached to the rear of the fuselage.

Surface-tuft photographs were made with a camera mounted outside the test section whereas tuft-grid photographs (see reference 5 for details of tuft-grid procedure) were made with an aerial camera mounted in the tunnel about 50 feet downstream of the model. The surface tufts were attached to the wing surface $\frac{1}{2}$-inch apart with cellulose tape along the following chord lines: 0, 0.05, 0.15, 0.25, 0.35, 0.45, 0.55, 0.70, 0.85, and 1.00. The tufts in the tuft grid were 3 inches long and were spaced at 1-inch intervals vertically and horizontally.

Force tests, wake surveys, surface-tuft tests, and tuft-grid tests were made for the various model arrangements shown in table I. The force tests consisted of measurements of lift, drag, and pitching moment through an angle-of-attack range of -6° to 39°. The wake surveys consisted of measurements of downwash and sidewash angles and dynamic pressure at the horizontal tail through the angle-of-attack range. The locations of these surveys are shown in figure 2. Surface-tuft and tuft-grid tests were made for a limited angle-of-attack range.

All force tests and wake surveys were made at a dynamic pressure of 39.7 pounds per square foot which corresponds to a Mach number of 0.17 and a Reynolds number of 1.1×10^6. The surface-tuft photographs were taken at a dynamic pressure of 24.9 pounds per square foot $\left(R = 0.885 \times 10^6\right)$ and the tuft-grid photographs were taken at a dynamic pressure of 8 pounds per square foot $\left(R = 0.493 \times 10^6\right)$.

CORRECTIONS

Approximate jet-boundary corrections, based on unswept-wing concepts, have been applied to the angle of attack and drag coefficient. The methods of reference 6, also for unswept wings, were used to determine blockage corrections which were applied to the drag coefficient and dynamic pressure. Corrections to horizontal-tail-on pitching moments and to the measured downwash angles were determined by the methods of reference 7. Support-strut tares have not been applied to the data but, with the exception of the drag tare, are believed to be small. The

[redacted]

absolute values of the drag coefficient are not believed to be representative of free-air conditions but the increments due to the various chord discontinuities are believed to be reliable.

RESULTS AND DISCUSSION

Presentation of Data

Table I is presented as an index to the figures with each model configuration designated by a number which will be used hereinafter. The following table summarizes the presentation of results of the present paper:

	Figures
Force data	5 to 15
Flow characteristics - Wake surveys	16 to 20
Flow characteristics - Surface tufts and tuft grid	21 and 22

Physical Nature of Flow

The physical nature of the flow over the surface of the wing and in the wake will be treated in this section, with reference to figures 21 and 22, to enable a better understanding of the force data. The effects of the fence and chord discontinuities on the flow will also be considered. Additional discussion of the flow will be made in a subsequent section of this paper.

At low angles of attack, visual observations of a tuft attached to a long slender rod indicated the presence of a vortex emanating near the wing-fuselage juncture of the basic complete model (configuration 1). This leading-edge separation vortex results from localized leading-edge separation and will be referred to hereinafter as the separation vortex. The separation vortex progressed along the leading edge of the wing to the tip, mixed with the tip vortex, and trailed downstream outboard of the horizontal tail. At angles of attack of about 6° to 8°, the separation vortex was swept from the wing leading edge (fig. 21) at about $0.68\frac{b_w}{2}$ and trailed off the wing to mix with the tip vortex, the mixed vortices passing outboard of the horizontal tail (fig. 22). At higher angles of attack, the separation vortex moved towards the plane of symmetry at the horizontal tail causing rapid changes in downwash angle.

[redacted]

The addition of a fence (extending around the wing leading edge and acting as a physical barrier to the separation vortex) having a length of 0.527c at $0.68\frac{b_w}{2}$ did not appreciably alter the flow over the wing (fig. 21) or in the wake at low angles of attack. At moderate angles of attack, however, the fence caused a definite improvement in the flow over the wing outboard of the fence. The improved flow outboard of the fence caused a higher tip loading compared with the flow over the plain wing at the same angle of attack thereby causing an increase in the stability of the wing.

The use of a chord-extension provides an aerodynamic barrier to the separation vortex in addition to a slight physical barrier. The aerodynamic barrier is a vortex along the inboard face (referred to as the face vortex) of the chord-extension and over the upper surface of the wing opposing the spanwise flow that otherwise exists from the separation vortex. When either a fence or chord-extension was on the wing, the tip vortex appeared to be stronger, a result of the improvement in flow outboard of these devices. A secondary vortex (emanating from the inboard face and the leading edge of the extension) was noted at high angles of attack along the leading edge of the chord-extensions.

The fence or chord-extension could appreciably alter the downwash characteristics at the horizontal tail as will be shown in a subsequent section of this paper.

Force Data

Lift and pitching moment.- The variation of lift and pitching-moment coefficient with angle of attack for several model configurations for the W, W + F + V, and W + F + V + H is shown in figure 5. It should be remembered that the angle of attack of the wing alone is referred to the fuselage center line (figs. 1 and 2) which is the reference line for configurations including a fuselage.

The data of figure 5(a) indicate that although the basic W + F + V + H (configuration 1) becomes longitudinally unstable at moderate angles of attack (about 10°), the W and W + F + V are stable in the same angle-of-attack range. The instability of the basic W + F + V + H was also the subject of the investigations of references 1 and 2. Tests of this same model (reference 2) with the wing removed indicated no appreciable decrease in stability around 10° angle of attack. It appears, then, that the aforementioned separation vortex has produced an unfavorable variation of downwash angle with angle of attack at the horizontal tail. Large increases in $\partial\epsilon/\partial\alpha$ to values as great as 2.0, with the dynamic

[redacted]

pressure at the tail remaining essentially equal to the free-stream value, are indicated for the moderate angle-of-attack range for configuration 1. (See fig. 16.)

A comparison of figures 5(a) to 5(d) indicates that the chord-extension (configuration 4) or fence (configuration 16) improves the stability of the W and W + F + V slightly in the angle-of-attack range where configuration 1 is unstable (W + F + V + H); the improvement in stability of the wing, however, is small compared to the improvement in stability of the complete model caused by the more favorable variation in downwash angle with angle of attack at the horizontal tail. (See fig. 16 for the variation of downwash angle with angle of attack for several spanwise positions at the horizontal tail for configurations 1 and 4.) The data of figure 16(b) indicate lower values of q_t/q for configuration 4 than for configuration 1 ($\alpha = 8^\circ$ to 12°) which would tend to reduce the instability caused by high values of $\partial\epsilon/\partial\alpha$ occurring for configuration 4 as well as configuration 1. Although downwash angles and q_t/q were not measured for configuration 16, they are believed similar to those of configuration 4 inasmuch as the pitching-moment data are very similar for the two configurations.

Comparisons of the effects of various chord discontinuities and some fence configurations on the stability and lift characteristics of the complete model (W + F + V + H) are presented in figures 6 to 13. In general, the chord discontinuities and fence configurations had very little effect on the lift and pitching moments at angles of attack less than about 10° and greater than about 25°. For intermediate angles of attack, the use of a chord-extension of $0.05\frac{b_w}{2}$ with the inboard face at $0.68\frac{b_w}{2}$ from the plane of symmetry (configuration 2) provides about neutral stability in the angle-of-attack range around 12° (resulting from favorable values of $\partial\epsilon/\partial\alpha$ (fig. 17)) but results in a small unstable range around 19° angle of attack (fig. 6) where $\partial\epsilon/\partial\alpha$ is greater than 1.0. The data of figure 6 also indicate that the effectiveness of the extension in improving the stability of the model is decreased by a small outboard displacement of the extension (configuration 3). The effect of increasing the span of the small extension (configurations 2 to 4) is an increase in the effectiveness and in the range of effectivenss of the extension (fig. 6).

Results of an investigation of the same basic model used in the present investigation reported in reference 2 indicated that lowering the horizontal tail from its present position (see fig. 2) to the fuselage center line resulted in neutral stability at about 10° angle of attack. In the present investigation, both the fence and the $0.10\frac{b_w}{2}$

[redacted]

chord-extension provided neutral stability in this angle-of-attack range. The mechanisms of the three methods to improve the stability are different, however. Lowering the horizontal tail moves it to a more favorable downwash region whereas the addition of a fence or chord-extension improves the downwash at the original tail position.

A chord-extension extending from $0.68\frac{b_w}{2}$ to the wing tip (configuration 7) affects the stability and lift characteristics of the complete model in a manner similar to that of the $0.10\frac{b_w}{2}$ chord-extension (configuration 4) having the inboard face at the same spanwise location. (Compare figs. 6 and 7.) Moving the face of the chord-extension outboard decreases the stability around 10° angle of attack.

In order to determine the influence of the profile of the inboard chord-extension on the lift and pitching-moment characteristics of configuration 4, a small flat-plate extension was investigated (configuration 6). The data of figure 8 indicate that the flat-plate extension is much less effective than the chord-extension of configuration 4 in reducing the instability that occurs at about 10° angle of attack for the basic complete model.

Generally, the effects of the fence (configuration 16) on the stability of the complete model are similar to those of the chord-extension of configuration 4 although the mechanism of the two devices differ considerably, as was previously mentioned. The fence was located at $0.68\frac{b_w}{2}$ as was the inboard face of the chord-extension. The chord-extension, however, was more effective in maintaining stability for a larger angle-of-attack range than was the fence (fig. 9).

A comparison of the effects of a single fence and multiple fences on the lift and pitching-moment characteristics of the complete model is presented in figure 10. In the angle-of-attack range around 10°, a single fence is much more effective in reducing the instability of the basic complete model (configuration 1) than the six fences investigated. For a small angle-of-attack range around 20°, the six fences are more effective than the single fence inasmuch as instability occurs for the single-fence configuration. At higher angles of attack, the single-fence configuration is more stable than the multiple-fence configuration.

When the chord discontinuity is in the form of a recessed chord outboard of $0.68\frac{b_w}{2}$ (configuration 10), only small effects of the discontinuity are noted on the lift and stability characteristics of the

[redacted]

basic complete model. (Compare figs. 10 and 11.) This is the result of a lack of an aerodynamic or physical barrier to the separation vortex. Moving the face of the recession outboard (decreasing span) does not appreciably alter the effectiveness of the recession nor does cambering the recession. (Compare figs. 11 and 12.) Although no improvement in stability is obtained by recessing the chord outboard of the extension of configuration 4 to form configuration 5, this latter configuration has better stability characteristics than a plain chord-recession because of the existence of the aerodynamic and physical barriers to the separation vortex. (Compare figs. 11 and 13.)

In general, chord-extensions were much more effective than chord-recessions in reducing the inherent instability of the basic complete model. This instability occurred near 10° angle of attack and was attributable to an unfavorable variation of downwash angle with angle of attack at the horizontal tail. The single fence was more effective than six fences for this angle-of-attack range and its effects on the instability of the basic W + F + V + H were comparable to those of the best chord-extension (configuration 4) (see fig. 9). Although some of the chord discontinuities investigated eliminated the instability of the plain complete model (configuration 1) near 10° angle of attack, none provided better than neutral stability in this range.

Drag.- The variation of drag coefficient with angle of attack for the basic W, W + F + V, and W + F + V + H model configurations is presented in figure 14. The variation of drag coefficient with angle of attack is presented in figure 15 for several chord-discontinuity configurations and a fence configuration. The chord-extension and fence configurations generally increase the drag coefficient at moderate and high angles of attack whereas the chord-recession slightly decreases the drag coefficient through the angle-of-attack range.

Flow Characteristics - Wake Surveys

The wake surveys (measurements of downwash angles, sidewash angles, and the dynamic pressures at the horizontal-tail location) were made along a line perpendicular to the plane of symmetry and passing through the 0.5 chord of the mean aerodynamic chord of the horizontal tail. A previous investigation (reference 1) had indicated the aerodynamic center of the tail to be near this point. Surveys were made in the plane of the horizontal tail only (tail removed) for configurations 1, 2, 4, 5, 7, and 10 and these data are presented in figures 16 to 20. Curves of the pitching-moment coefficient plotted against angle of attack for the complete model (W + F + V + H) are also included in these figures.

The data of figures 16 to 20 indicate that the downwash angle at the horizontal tail for all configurations varies considerably through

the angle-of-attack range at all spanwise stations investigated. At low angles of attack, $\partial\epsilon/\partial\alpha$ is fairly constant but begins to increase across the span at about $\alpha = 8^\circ$. At the outboard survey positions, a maximum value of $\partial\epsilon/\partial\alpha$ is reached at lower angles of attack than at the inboard survey positions. At low angles of attack, the value of $\partial\epsilon/\partial\alpha$ is generally less than 0.5 and at angles of attack between 8° and 16°, depending on the spanwise station, it becomes as large as 2.0 for some configurations.

The sidewash angles measured in the plane of the horizontal tail are shown in figures 16 to 20. Inasmuch as the angle of sideslip was zero for the present investigation, it can be expected that the sidewash angles on the other semispan would be approximately the same; thus, sidewash would not influence the static longitudinal stability.

For all configurations, the dynamic pressure at the horizontal-tail position is essentially equal to the free-stream value for low angles of attack and begins to decrease at some moderate angle of attack. The rate of decrease of q_t/q is greater for outboard stations and minimum values of q_t/q as low as 0.36 are obtained, the angle of attack for minimum q_t/q varying with the spanwise stations (figs. 16 to 20).

The configurations (2, 5, and 7) which have longitudinal stability characteristics similar to configuration 4 for the unstable angle-of-attack range of configuration 1 (about $\alpha = 9^\circ$ to 14°) generally have similar downwash and dynamic-pressure characteristics. (Compare figs. 17 to 19.) Configurations 1 and 10 have similar static longitudinal stability characteristics (figs. 10 and 11, respectively) and have about the same downwash and dynamic-pressure patterns (figs. 16 and 20, respectively).

Flow Characteristics - Surface Tufts and Tuft Grid

Surface-tuft photographs ($R = 0.885 \times 10^6$) are presented in figure 21 for several model configurations for the angle-of-attack range where instability occurred for configuration 1. Also presented in figure 21 are tuft-grid photographs ($R = 0.493 \times 10^6$) for several angles of attack for the wing alone for configuration 1. All angles of attack are referred to the fuselage center line. Inasmuch as there are only a few tuft-grid photographs at angles of attack comparable to the angles of attack for the surface-tuft photographs, figure 22 was prepared and includes intermediate and lower angles of attack to give a more complete wake pattern. The various chord-discontinuity and fence configurations did not show any appreciable change in the flow patterns distinguishable by casual observation of the photographs. The vortices on or along the

[redacted]

face of the chord-extensions were weak compared with the separation vortex and, thus, were masked from view at the horizontal-tail position. Hence, only tuft-grid photographs are presented for configuration 1.

Configuration 1, plain wing.- Inasmuch as the physical nature of the flow has been discussed in a previous section, only brief consideration to additional details will be discussed herein.

The inboard movement of the separation vortex becomes apparent from the photographs in figures 21 and 22 for angles of attack above 9° in the form of a distorted vortex pattern. As the angle of attack is increased, the separation vortex becomes progressively larger and moves farther inboard. Vorticity is apparent behind almost the entire wing. Probing at the horizontal tail location indicated very rough flow.

Configuration 16, fence at $0.68\frac{b_w}{2}$.- In order to determine whether spanwise position of the fence would be critical with regard to its effectiveness in improving the flow over the wing surface, observations of the surface tufts were made with a fence probe located at different positions along the wing. The fence probe consisted of fence 4 (fig. 3) attached to a long slender rod. As the fence probe was moved inboard of $0.68\frac{b_w}{2}$, no appreciable improvement in the flow outboard of the fence was noted. Moving the fence outboard of $0.68\frac{b_w}{2}$ showed some improvement in the flow outboard of the fence but the range of angles of attack for a continued improvement in flow was severely curtailed.

Apparently, in order to be highly effective for a large angle-of-attack range, the fence should be located very close to the point where the separation vortex begins to sweep backward from the wing leading edge which usually occurs at some moderate angle of attack. In addition, the fence should extend to, or around, the wing leading edge. Addition of slots or flaps to the wing, or a change in wing aspect ratio, would alter the vortex behavior and would, therefore, influence the optimum location of the fence (reference 1) as, perhaps, would Reynolds number.

Chord discontinuities.- Probing at low angles of attack (about 3°) with the $0.10\frac{b_w}{2}$ chord-extension (configuration 4) on the wing indicated the presence of vortices along the inboard and outboard faces of the chord-extension. These face vortices are more or less evident from the disturbances of the surface tufts in these regions (fig. 21). The outboard face vortex was weak and, although it may have become stronger at higher angles of attack, it is believed that the effects of this vortex would be relatively small in comparison to the other vortices. Even at an angle of attack of 21°, the flow over the extension was relatively smooth.

[redacted]

Incidentally, probing indicated a region of very low dynamic pressure inboard of the chord-extension at about 35 percent of the wing chord at an angle of attack of 7°. This region is indicated by the apparent bare spot among the tufts (fig. 21).

The tuft photographs are generally similar in nature for the $0.32\frac{b_w}{2}$ chord-extension (configuration 7) as for the $0.10\frac{b_w}{2}$ chord-extension (configuration 4). (See fig. 21.) The use of the large chord-extension moves the entire leading edge outboard of the discontinuity out of the path of the separation vortex. The vortex along the face of the chord-extension tends to reduce the effects of the separation vortex. At high angles of attack, the formation of a secondary vortex along the leading edge of the chord-extension is apparent from the photographs of figure 21. The effects on the flow of recessing the chord of the wing outboard of $0.68\frac{b_w}{2}$ can also be seen in figure 21. The flow is similar to that for the plain wing as might be expected since no aerodynamic or physical barriers exist to counteract the effects of the separation vortex. In fact, the vortex on the face of the recession rotates in the same direction as the separation vortex and, thus, tends to magnify the unstable flow at the horizontal tail caused by the separation vortex. The recession also effectively increases the rate of taper (decreases the taper ratio) which would tend to increase the spanwise flow. As a result, the recession was ineffective in decreasing the instability of the plain wing configuration (W + F + V + H) as was previously noted.

CONCLUSIONS

A low-speed investigation to determine the effects of chord discontinuities and chordwise fences on the static longitudinal stability and wake characteristics of a swept-wing model has indicated the following conclusions:

1. The use of a fence or 10-percent-semispan chord-extension, with the inboard face of the chord-extension located at the same spanwise location as the fence (0.68 semispan), caused a slight improvement in the static longitudinal stability of the basic wing alone at moderate angles of attack which resulted from an improvement in flow over the tip of the wing and higher tip loadings for a given angle of attack.

2. A fence located at 0.68 semispan or a 0.10-percent-semispan chord-extension with the inboard face located at 0.68 semispan reduced the instability of the complete model to neutral stability at moderate angles of attack. The fence acted as a physical barrier to the

leading-edge separation vortex, thereby improving the flow over the wing outboard of the fence. The fence, however, mainly provided a more favorable variation of downwash angle with angle of attack at the horizontal tail. The chord-extension provided an aerodynamic barrier to the leading-edge separation vortex in the form of a vortex along the inboard face of the extension and, in addition, it provided a slight physical barrier to the separation vortex. The chord-extension also mainly provided a more favorable variation of downwash angle with angle of attack at the horizontal tail.

3. The chord-recessions investigated did not appreciably reduce the instability of the basic complete model because of the lack of a physical or aerodynamic barrier to the separation vortex.

Langley Aeronautical Laboratory
National Advisory Committee for Aeronautics
Langley Field, Va.

REFERENCES

1. Queijo, M. J., and Jaquet, Byron M.: Wind-Tunnel Investigation of the Effect of Chordwise Fences on Longitudinal Stability Characteristics of an Airplane Model With a 35° Sweptback Wing. NACA RM L50K07, 1950.

2. Queijo, M. J., and Wolhart, Walter D.: Wind-Tunnel Investigation of the Effects of Horizontal-Tail Position on the Low-Speed Longitudinal Stability Characteristics of an Airplane Model With a 35° Sweptback Wing Equipped With Chordwise Fences. NACA RM L51H17, 1951.

3. Lowry, John G., and Schneiter, Leslie E.: Investigation at Low Speed of the Longitudinal Stability Characteristics of a 60° Swept-Back Tapered Low-Drag Wing. NACA TN 1284, 1947.

4. Furlong, G. Chester: Exploratory Investigation of Leading-Edge Chord-Extensions to Improve the Longitudinal Stability Characteristics of Two 52° Sweptback Wings. NACA RM L50A30, 1950.

5. Bird, John D., and Riley, Donald R.: Some Experiments on Visualization of Flow Fields Behind Low-Aspect-Ratio Wings by Means of a Tuft Grid. NACA TN 2674, 1952.

6. Herriot, John G.: Blockage Corrections for Three-Dimensional-Flow Closed-Throat Wind Tunnels, With Consideration of the Effect of Compressibility. NACA Rep. 995, 1950. (Supersedes NACA RM A7B28.)

7. Gillis, Clarence L., Polhamus, Edward C., and Gray, Joseph L., Jr.: Charts for Determining Jet-Boundary Corrections for Complete Models in 7- by 10-Foot Closed Rectangular Wind Tunnels. NACA ARR L5G31, 1945.

[redacted]

TABLE I - INDEX TO FIGURES

No.	Plan view	Components investigated	Figure: Force tests	Figure: Wake surveys	Figure: Surface tufts	Figure: Tuft grid
1	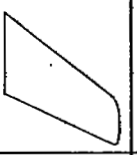	W W+F+V W+F+V+H	5,6 8-10 13-15	16	21	21 22
2	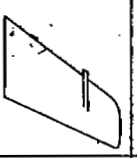	W+F+V+H	6	17	—	—
3	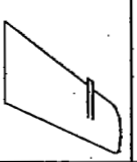	W+F+V+H	6	—	—	—
4	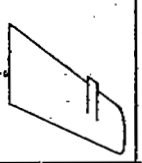	W W+F+V W+F+V+H	5 6, 8 9, 13 15	16-19	21	—
5	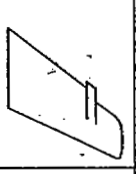	W+F+V+H	13	18 20	—	—
6	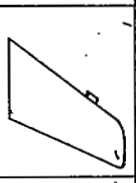	W+F+V+H	8	—	—	—
7	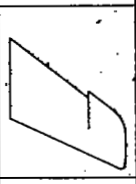	W+F+V+H	7, 15	19	21	—
8	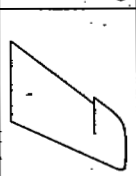	W+F+V+H	7	—	—	—

No.	Plan view	Components investigated	Figure: Force tests	Figure: Wake surveys	Figure: Surface tufts	Figure: Tuft grid
9	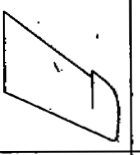	W+F+V+H	7	—	—	—
10	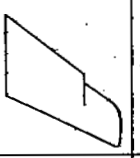	W+F+V+H	11 15	20	21	—
11	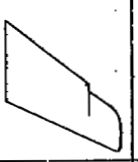	W+F+V+H	11	—	—	—
12	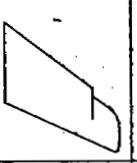	W+F+V+H	11	—	—	—
13	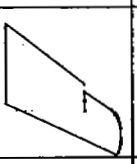	W+F+V+H	12	—	—	—
14	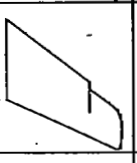	W+F+V+H	12	—	—	—
15	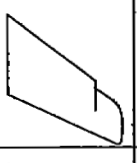	W+F+V+H	12	—	—	—
16	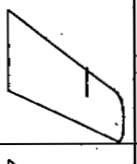	W W+F+V W+F+V+H	5 9, 10 15	—	—	—
17	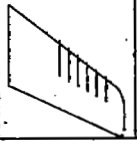	W W+F+V W+F+V+H	5 10	—	—	—

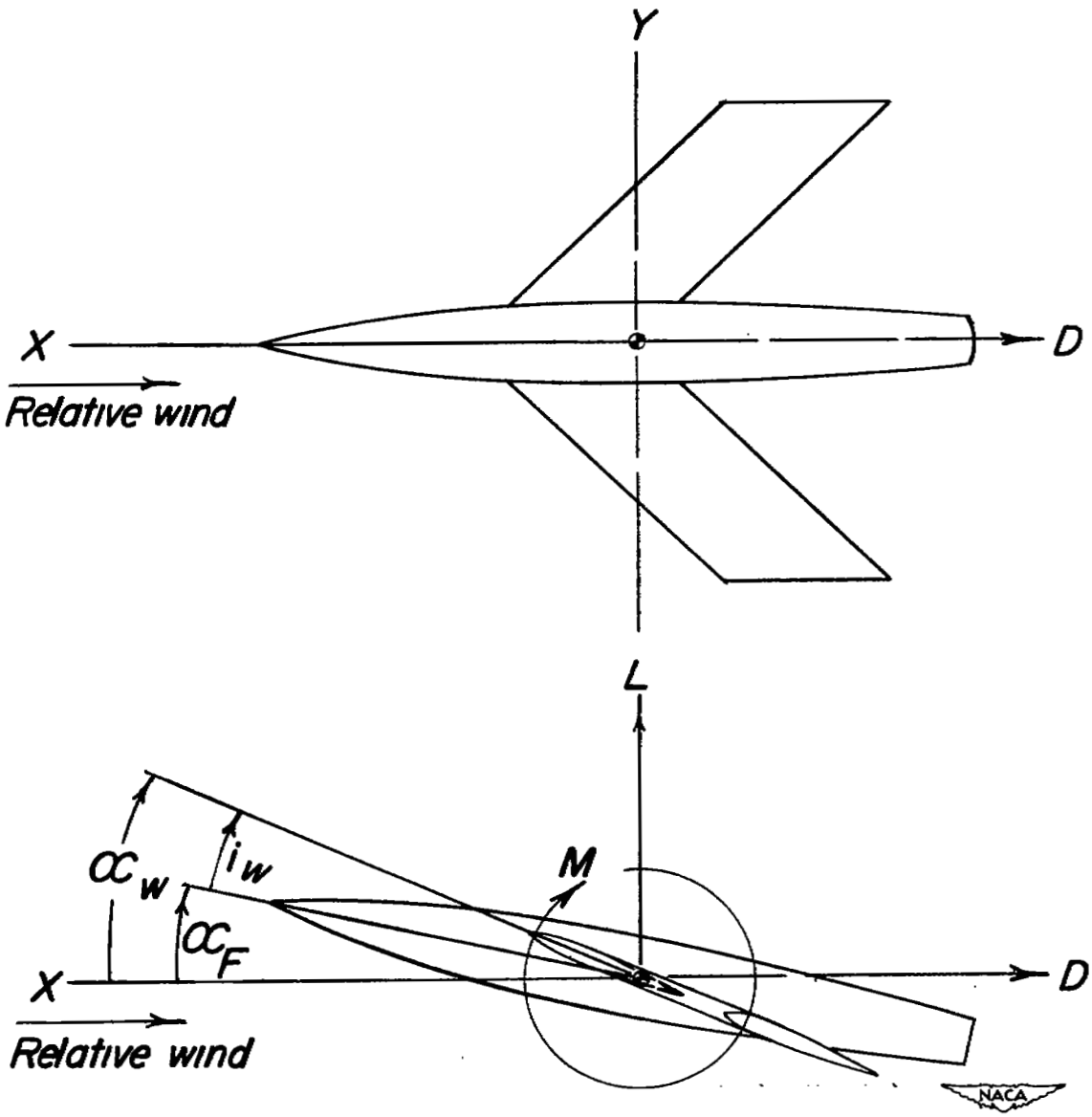

Figure 1.- Stability system of axes. Arrows indicate positive direction of forces, moments, and angular displacements.

[redacted]

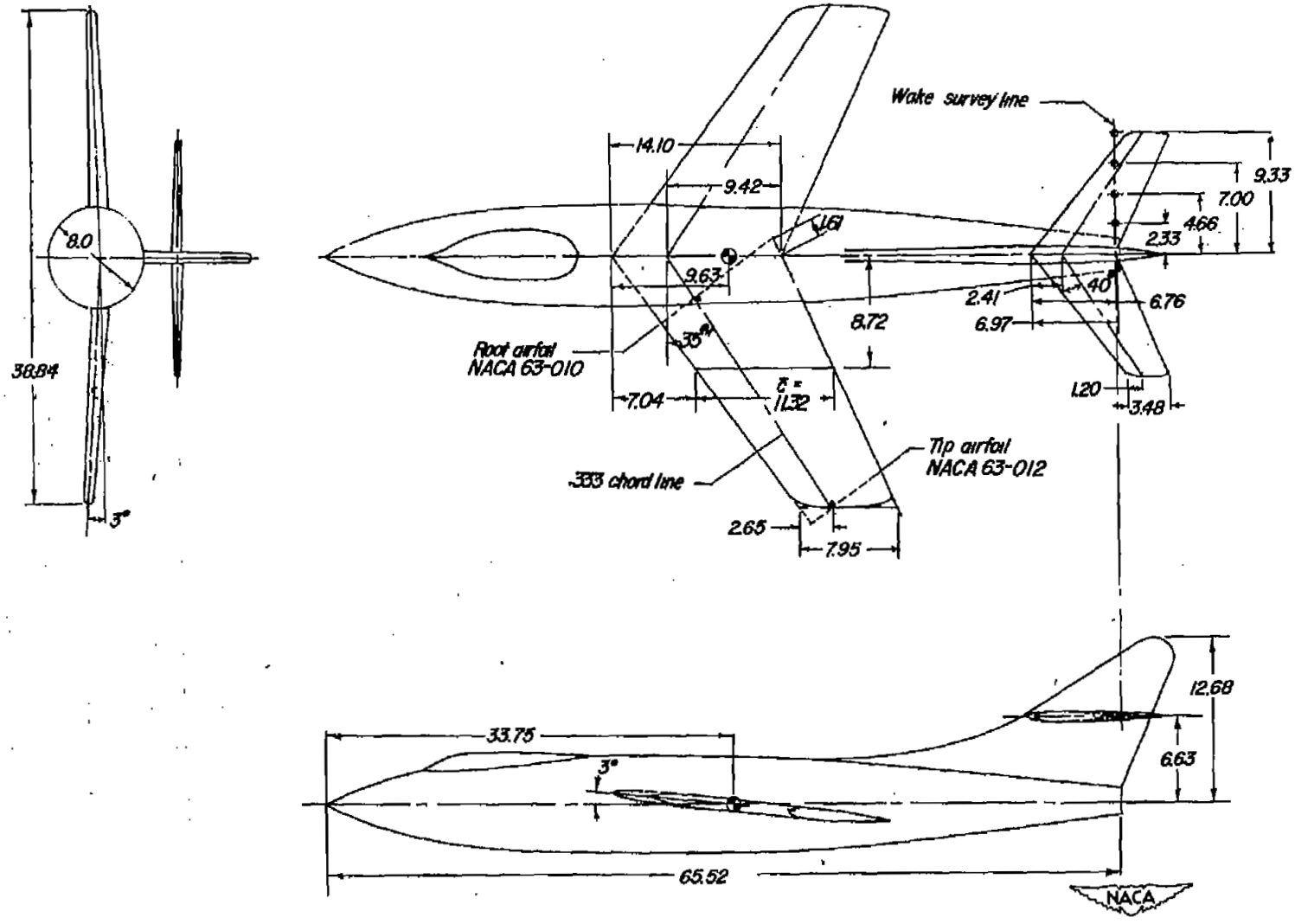

Figure 2.- Pertinent model dimensions. Configuration 1. All dimensions are in inches.

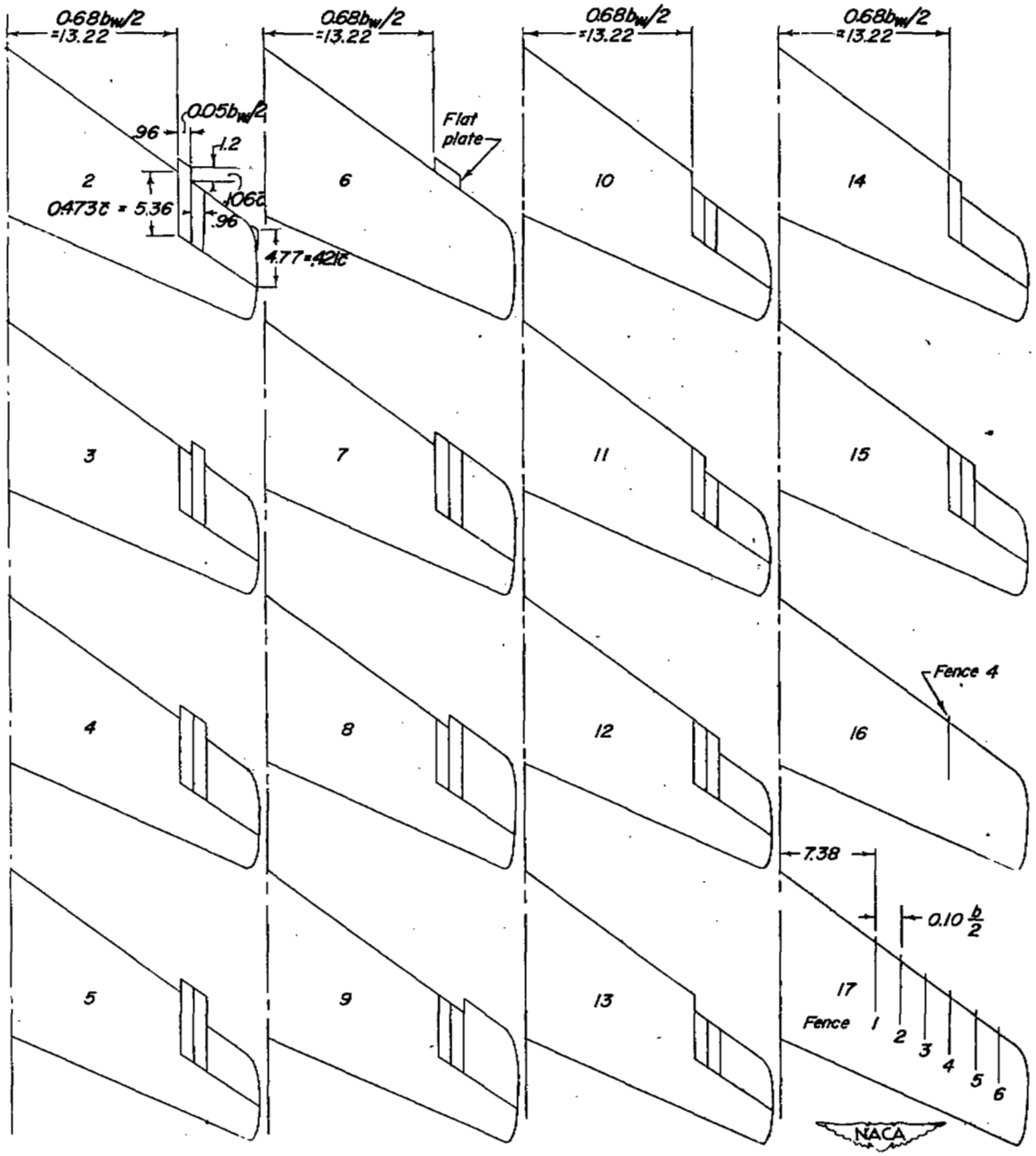

Figure 3.- Details of chord discontinuities and chordwise fences used in investigation. All dimensions are in inches. (Note: Recession in 13, 14, and 15 is cambered. See fig. 3 concluded.)

[redacted]

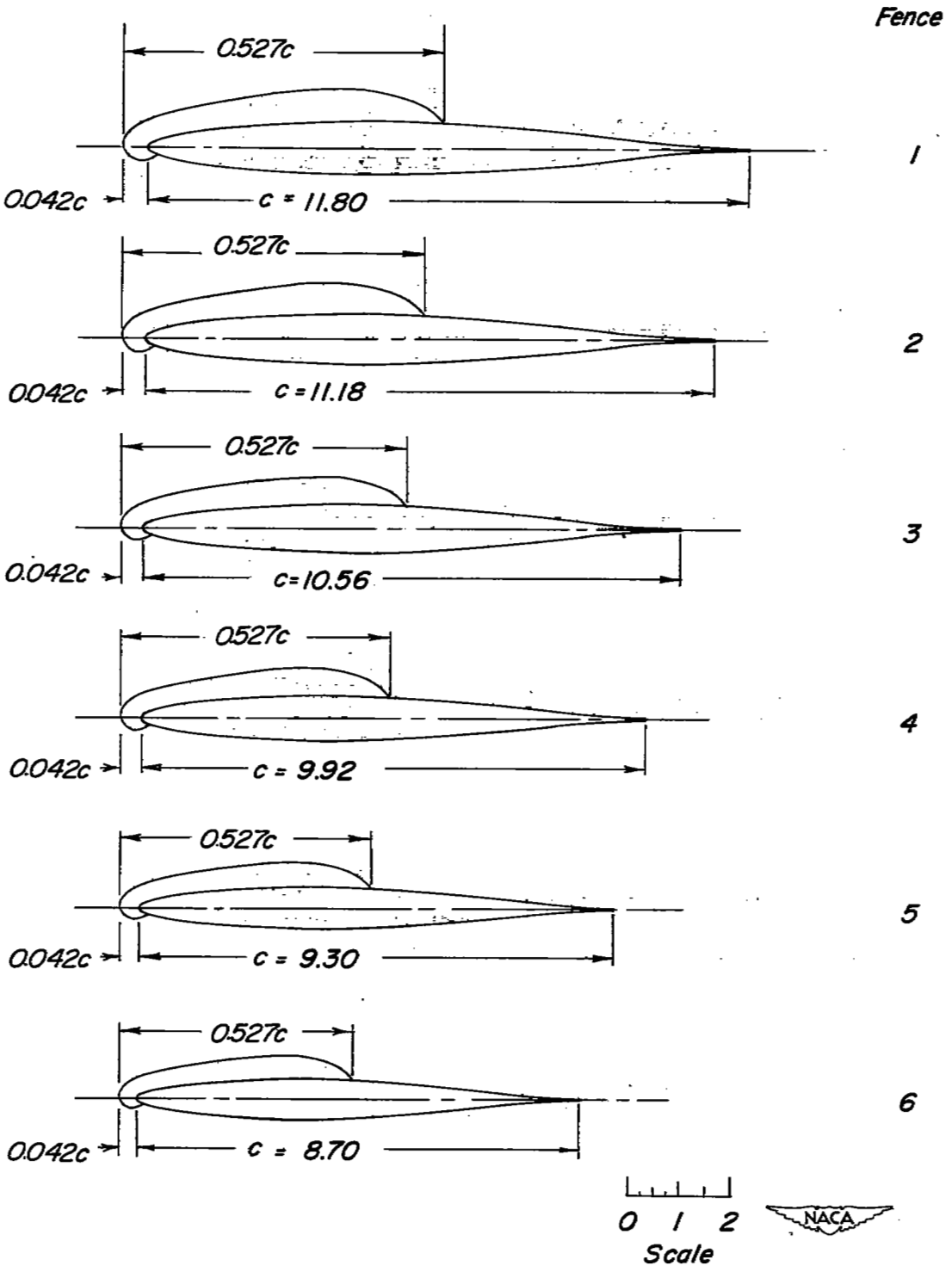

Figure 3.- Continued.

[redacted]

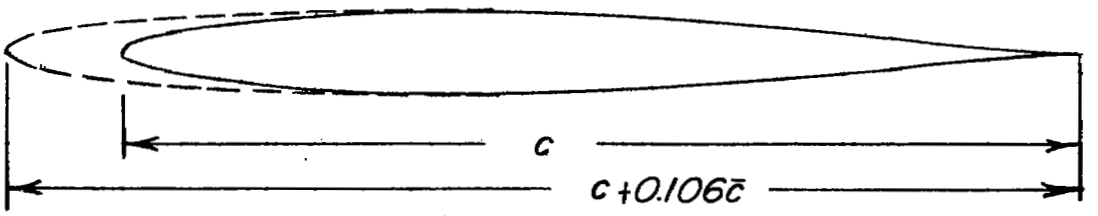

Typical extended leading edge

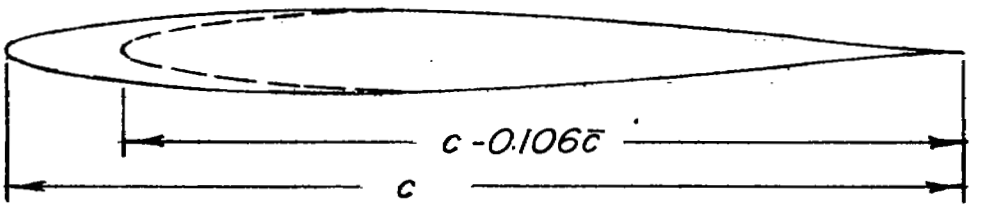

Typical recessed leading edge

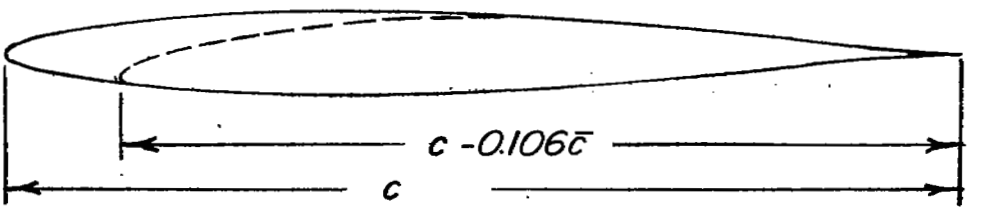

Typical combered – recessed leading edge

Figure 3.- Concluded.

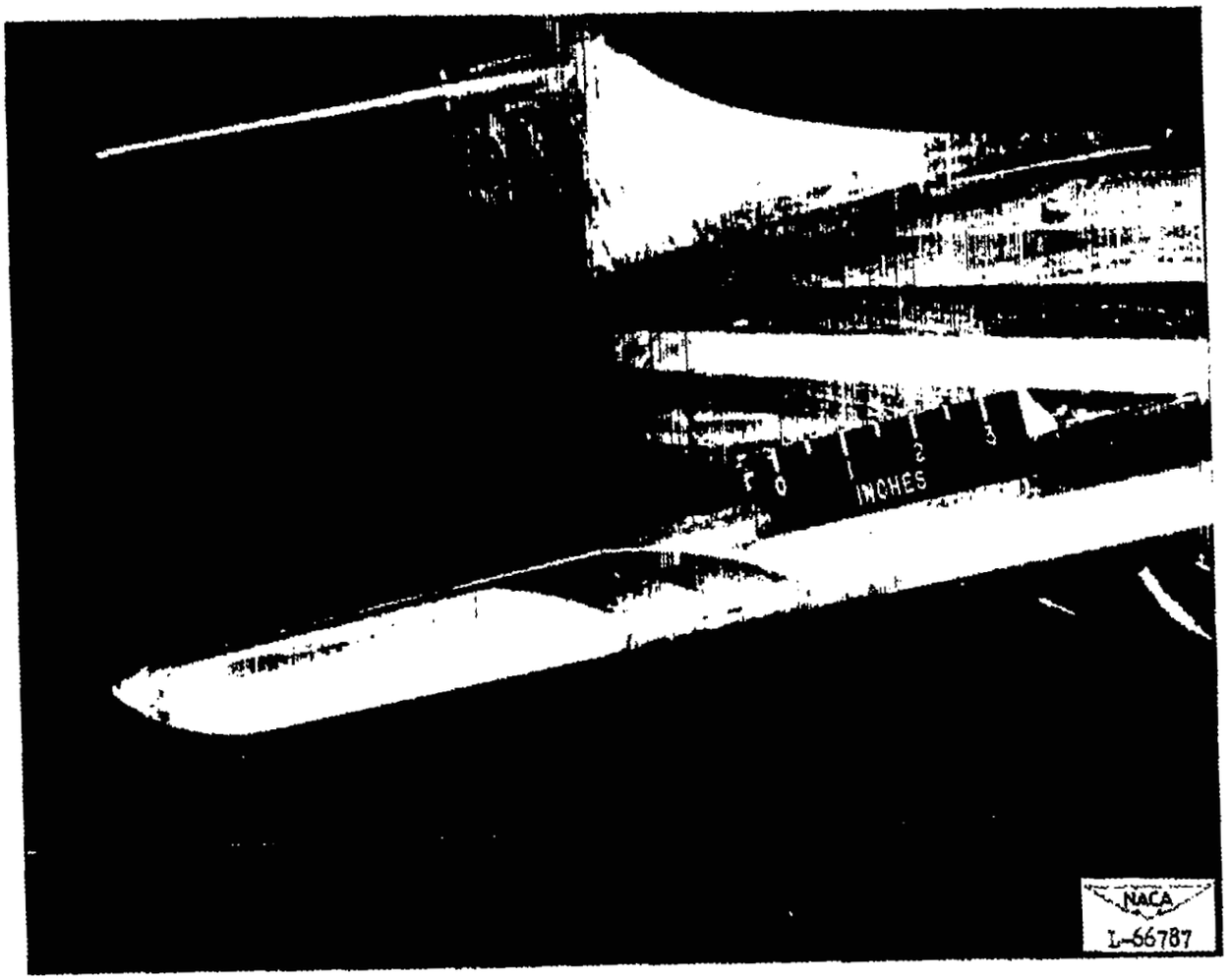

(a) Configuration 1.

Figure 4.- Photographs of various model configurations.

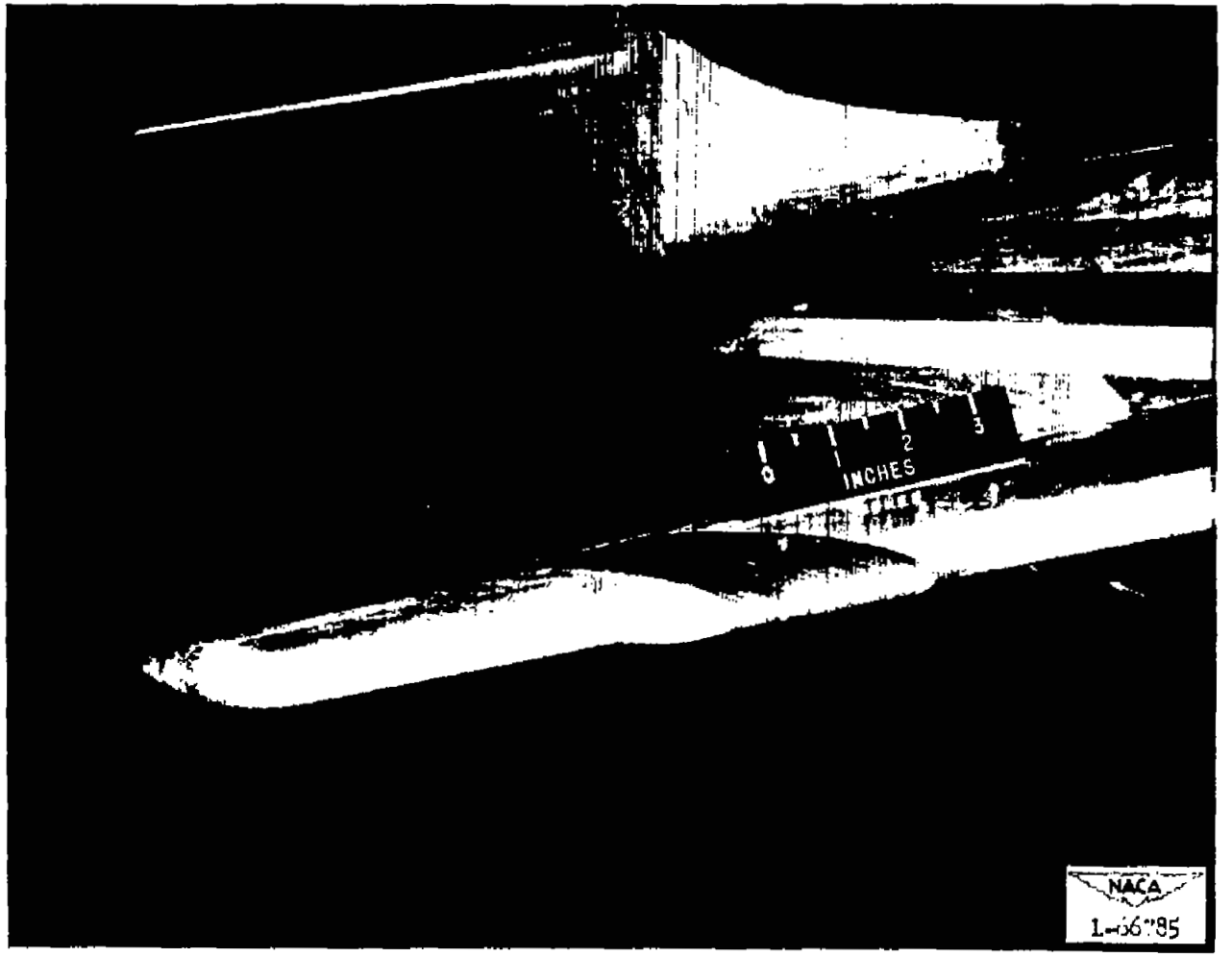

(b) Configuration 4.

Figure 4.- Continued.

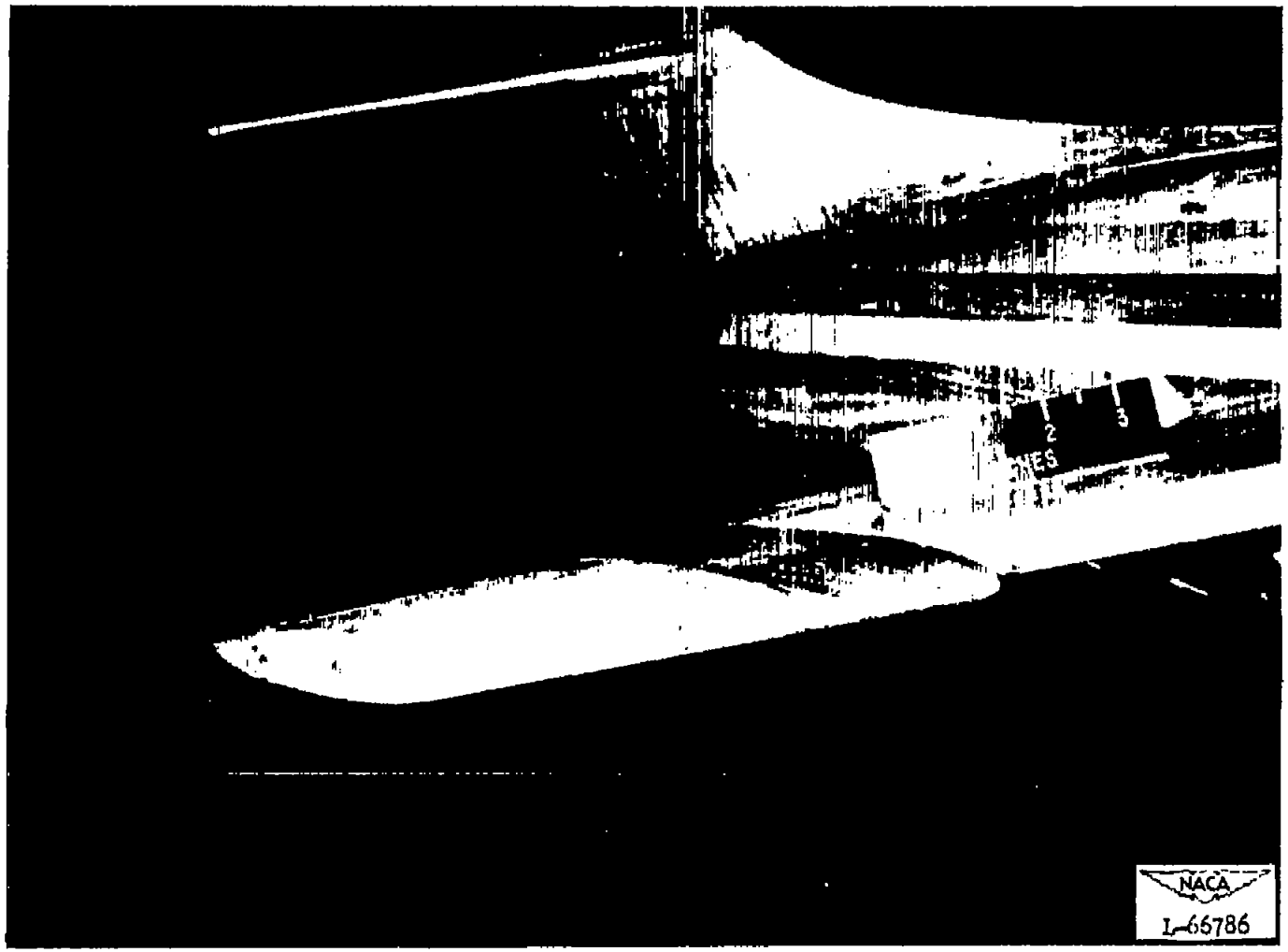

(c) Configuration 7.

Figure 4.- Continued.

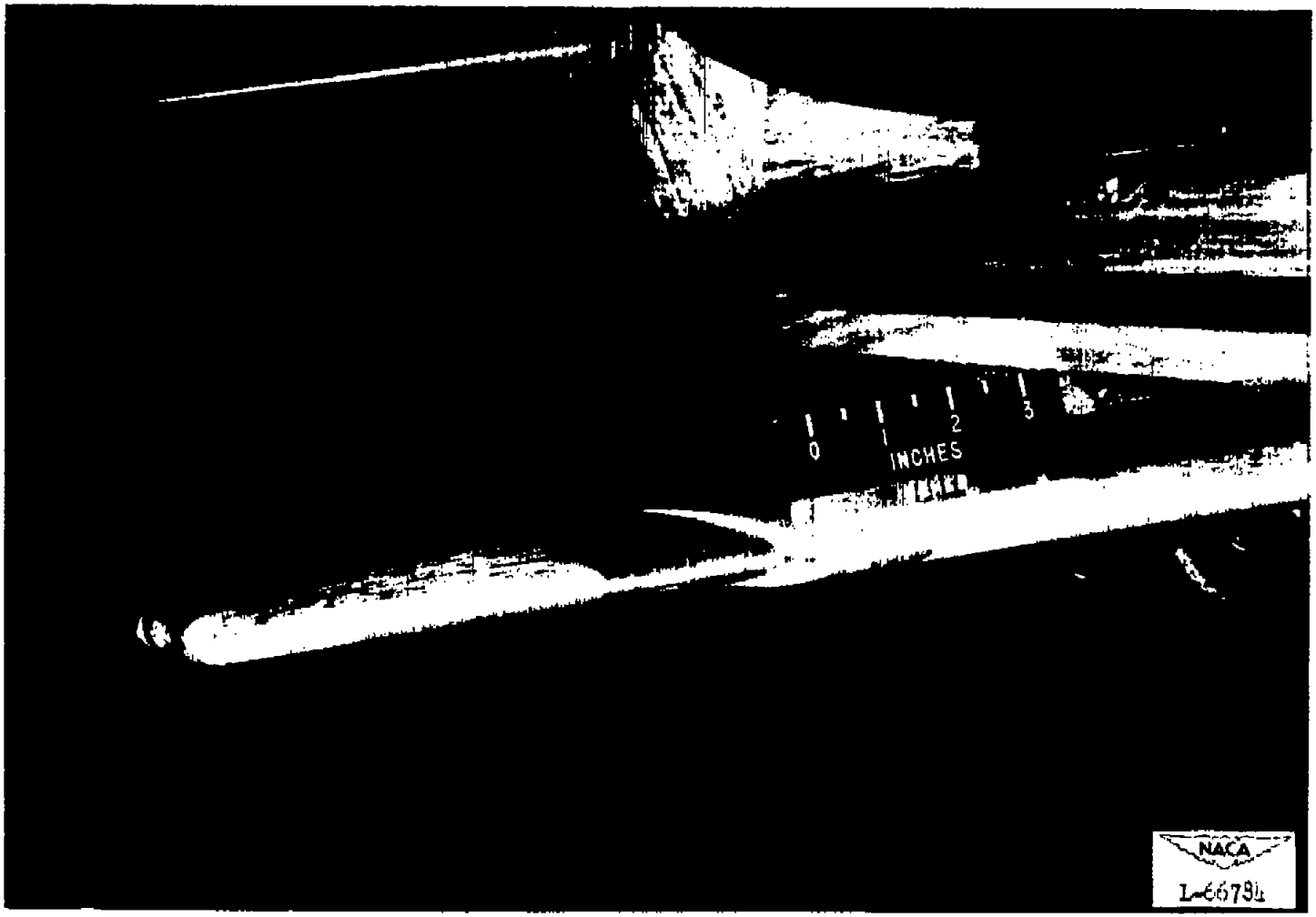

(d) Configuration 10.

Figure 4.- Continued.

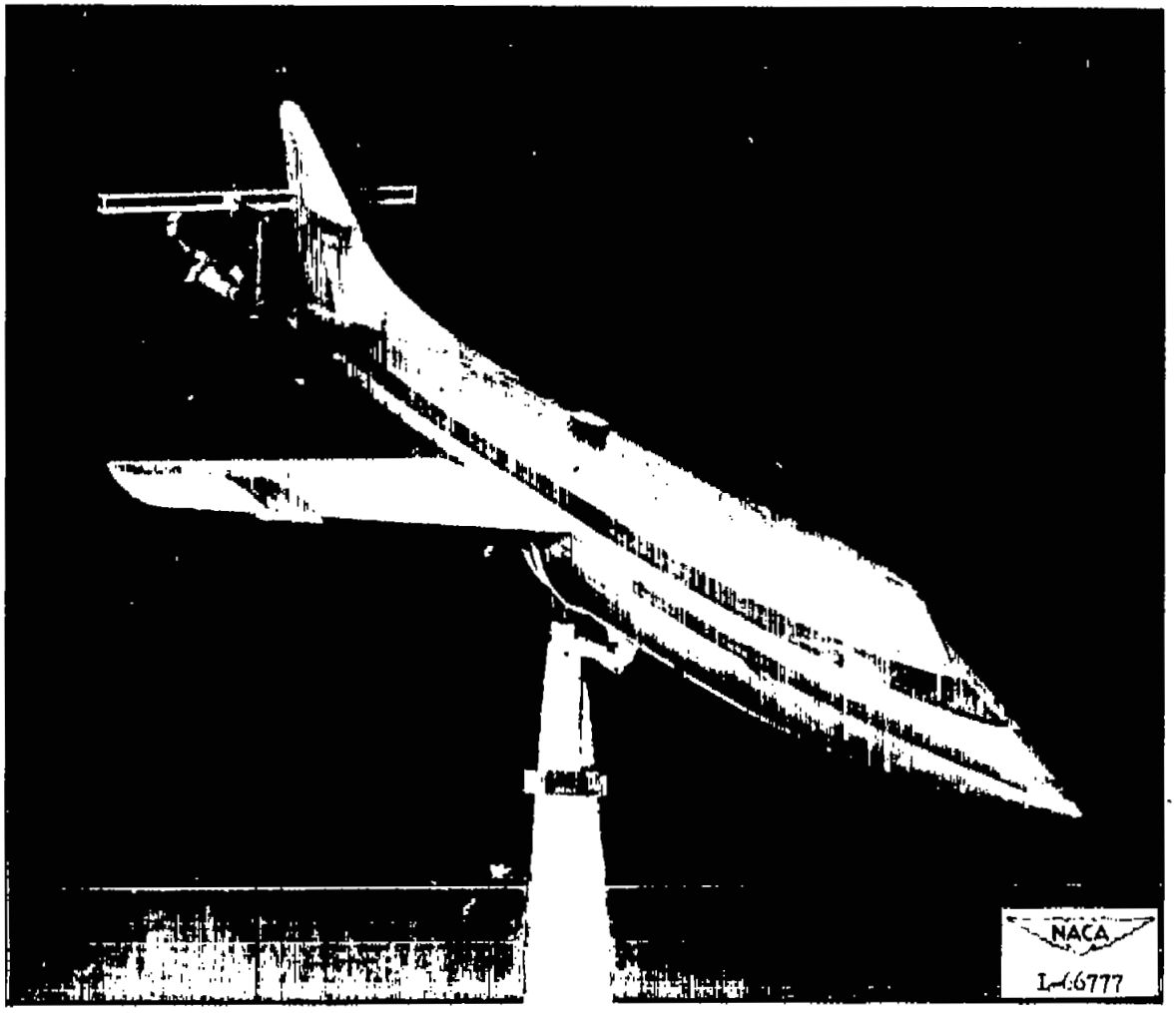

(e) Three-quarter front view of configuration 4 with survey apparatus attached.

Figure 4.- Concluded.

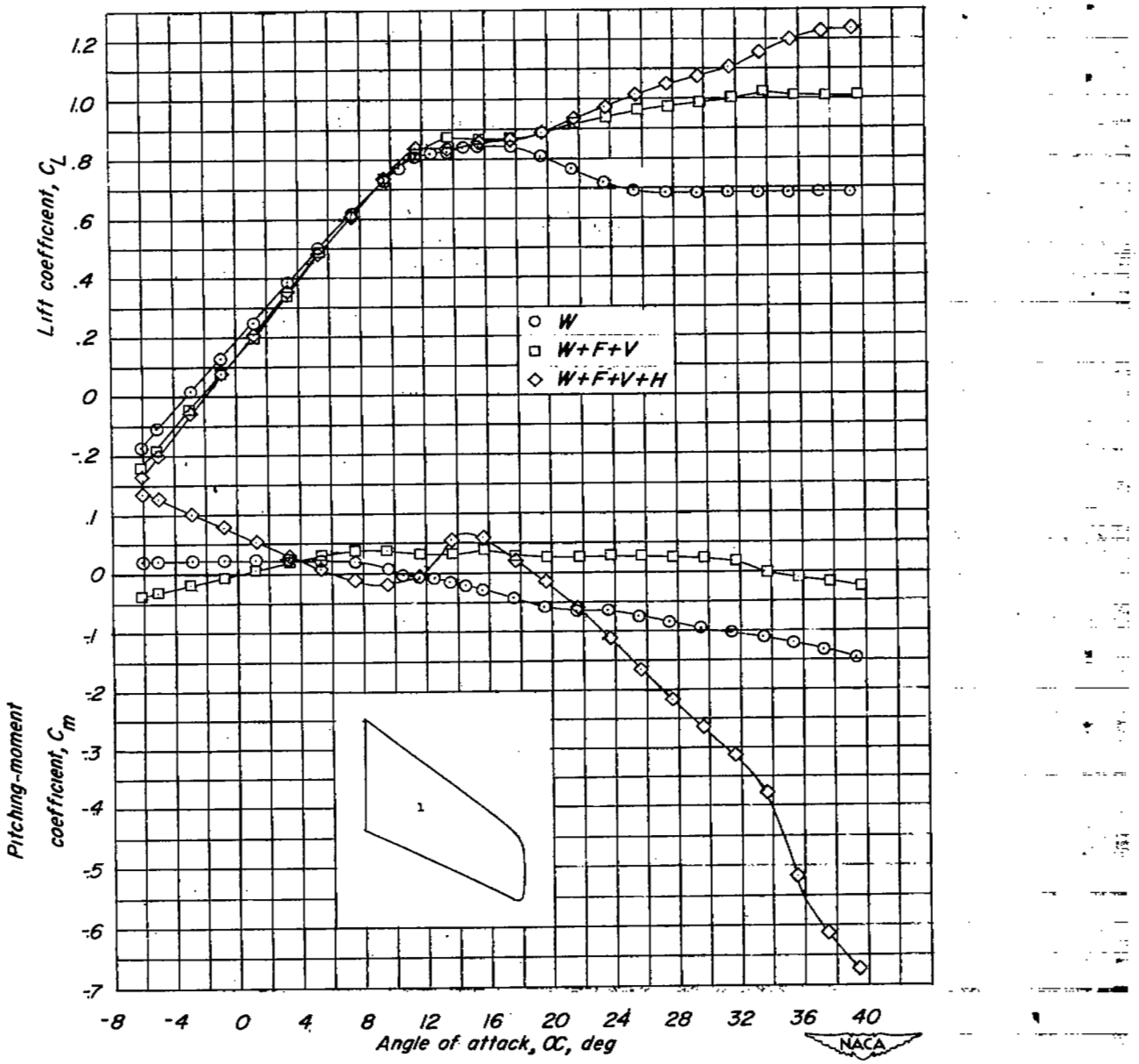

(a) Configuration 1.

Figure 5.- Longitudinal stability characteristics of an airplane model having a 35° sweptback wing.

[redacted]

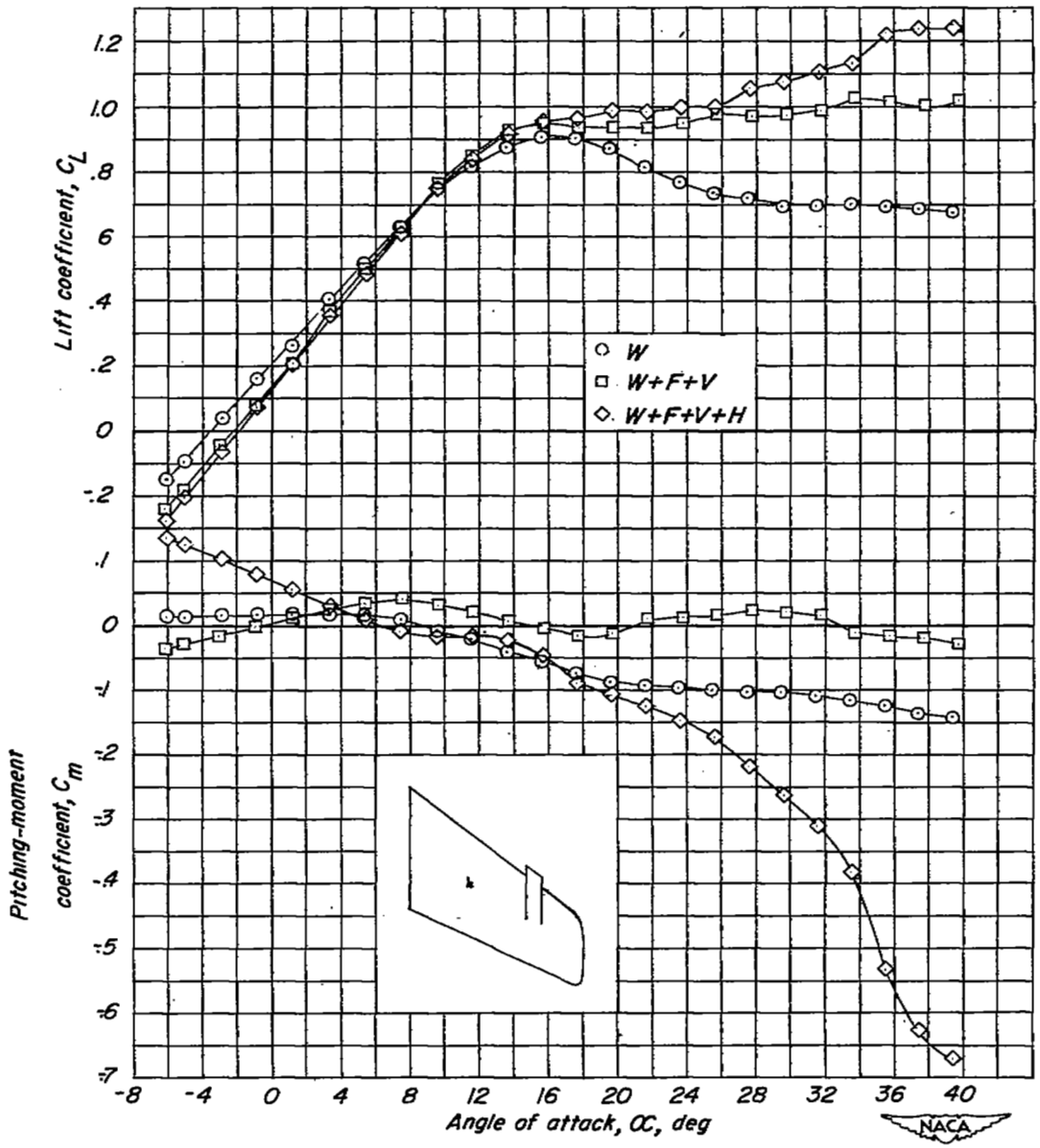

(b) Configuration 4.

Figure 5.- Continued.

[redacted]

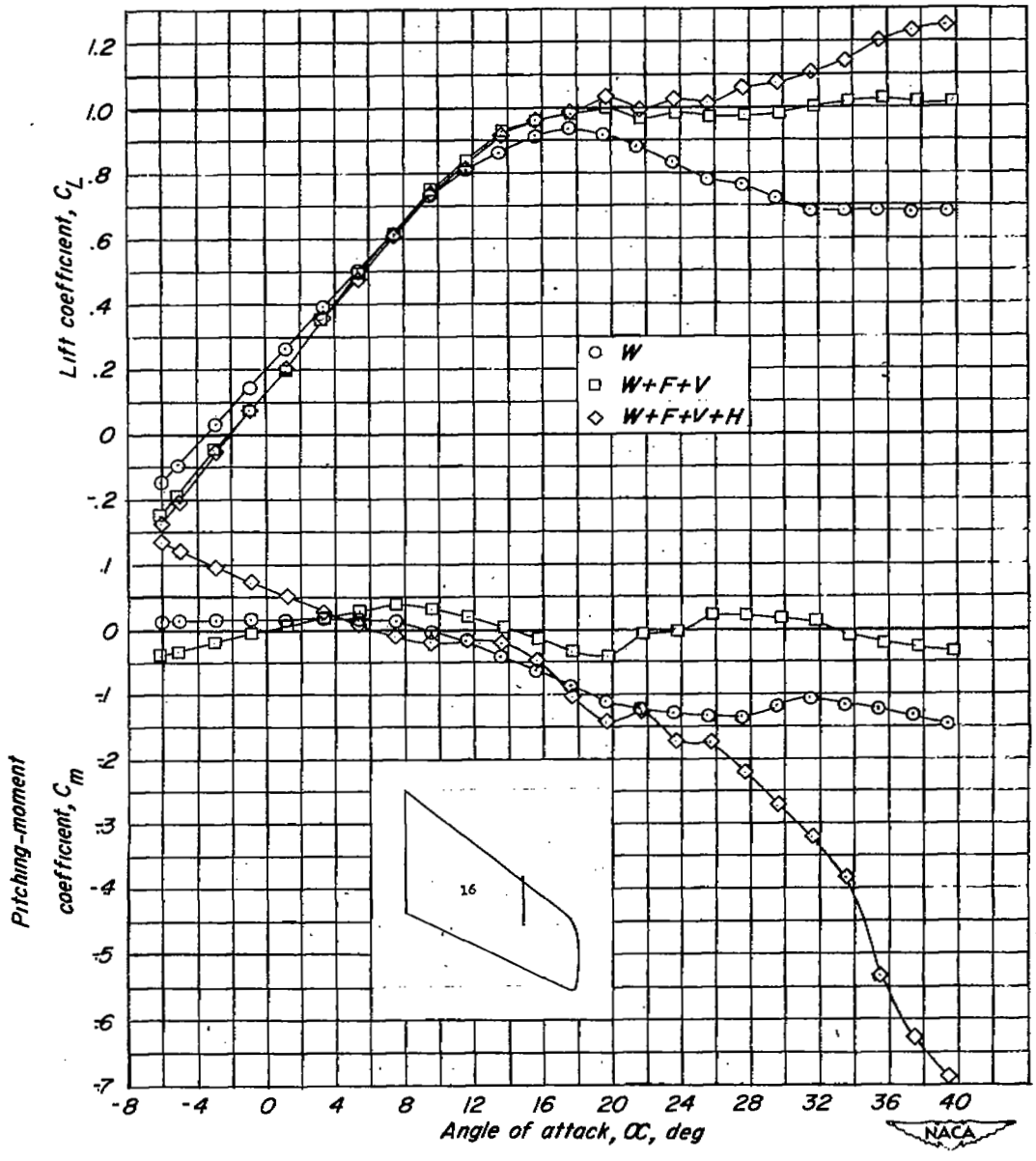

(c) Configuration 16.

Figure 5.- Continued.

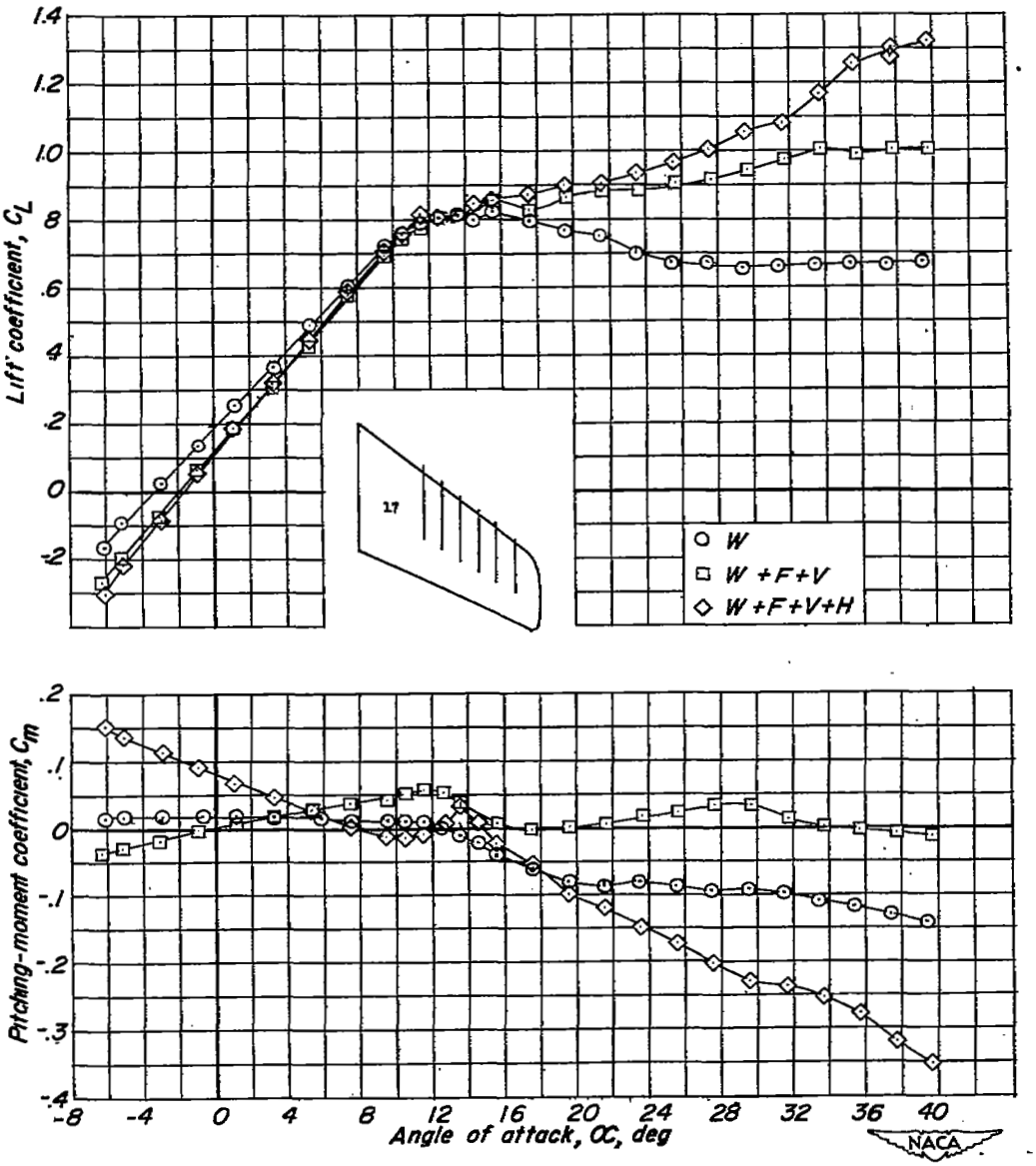

(d) Configuration 17.

Figure 5.- Concluded.

[redacted]

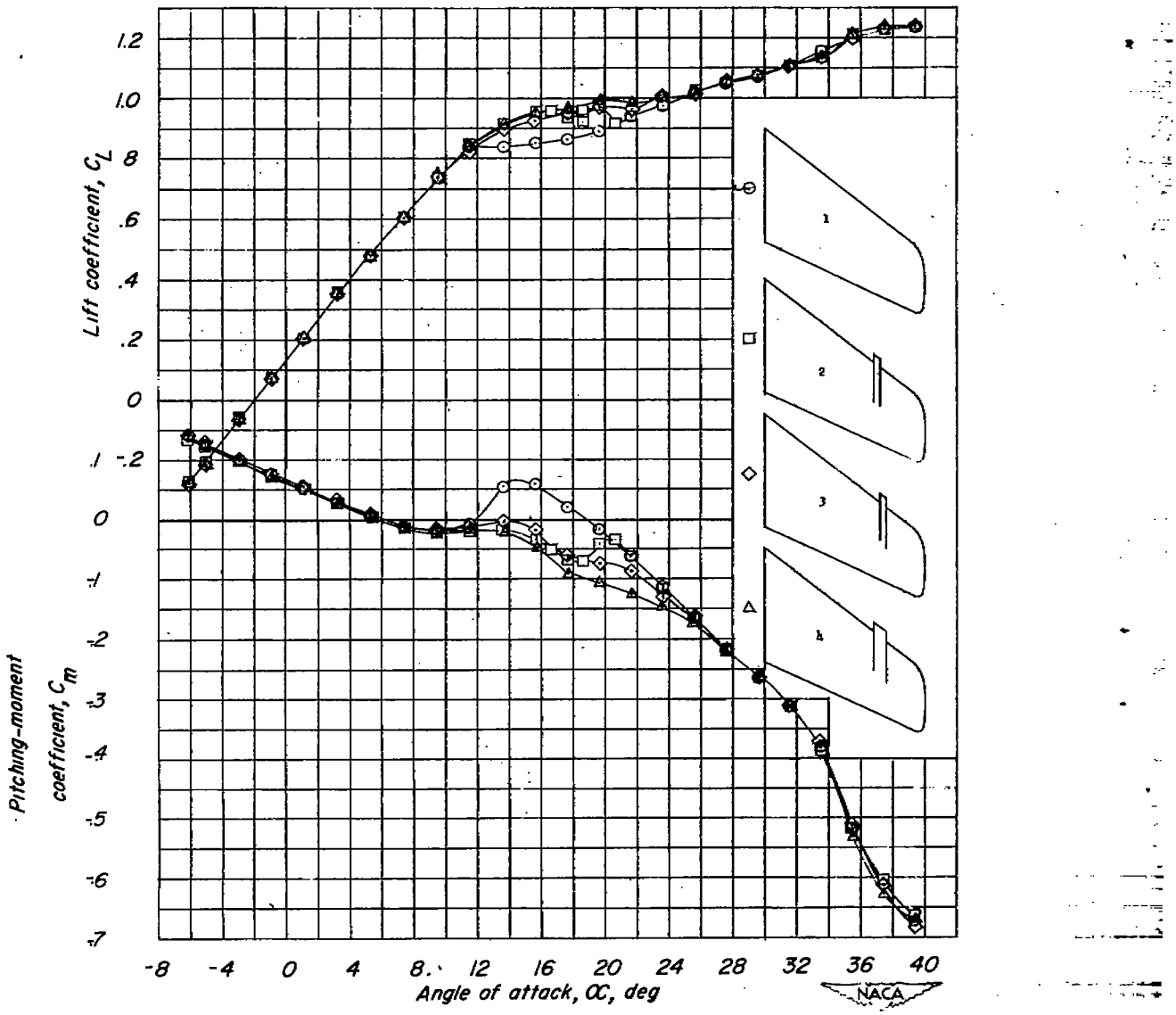

Figure 6.- Comparison of longitudinal stability characteristics of several model configurations. W + F + V + H.

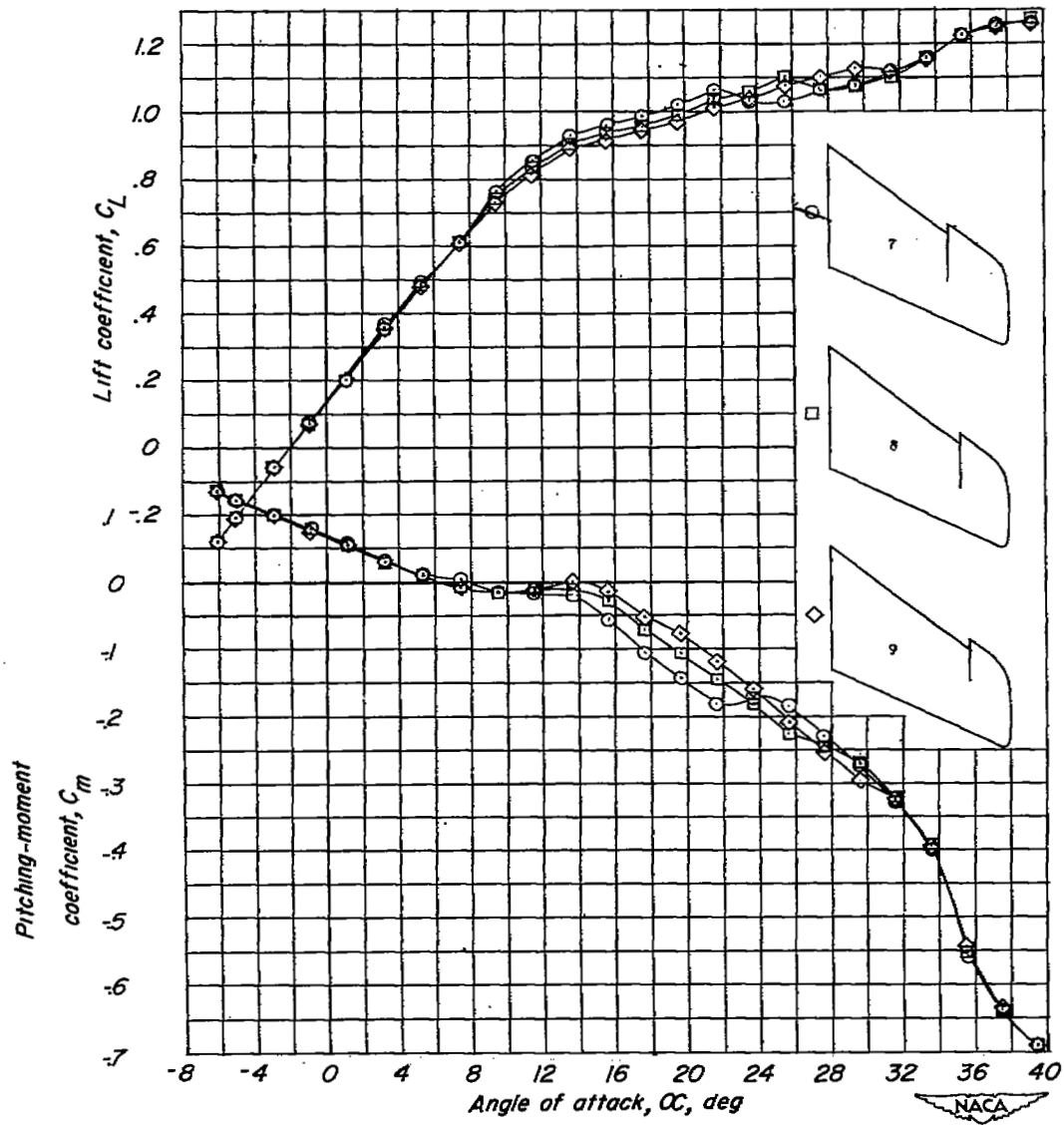

Figure 7.- Comparison of longitudinal stability characteristics of several model configurations. W + F + V + H.

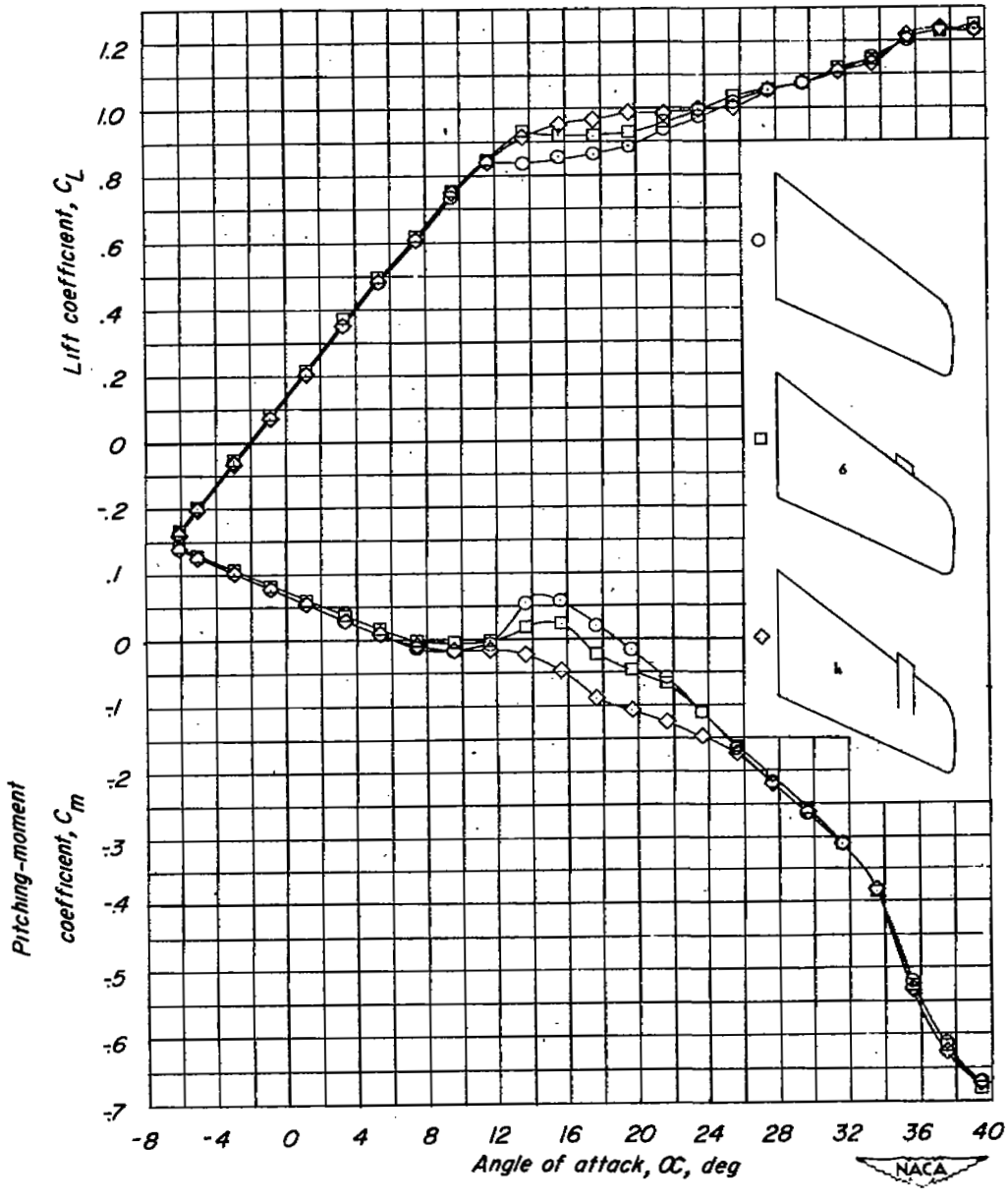

Figure 8.- Comparison of longitudinal stability characteristics of several model configurations. W + F + V + H.

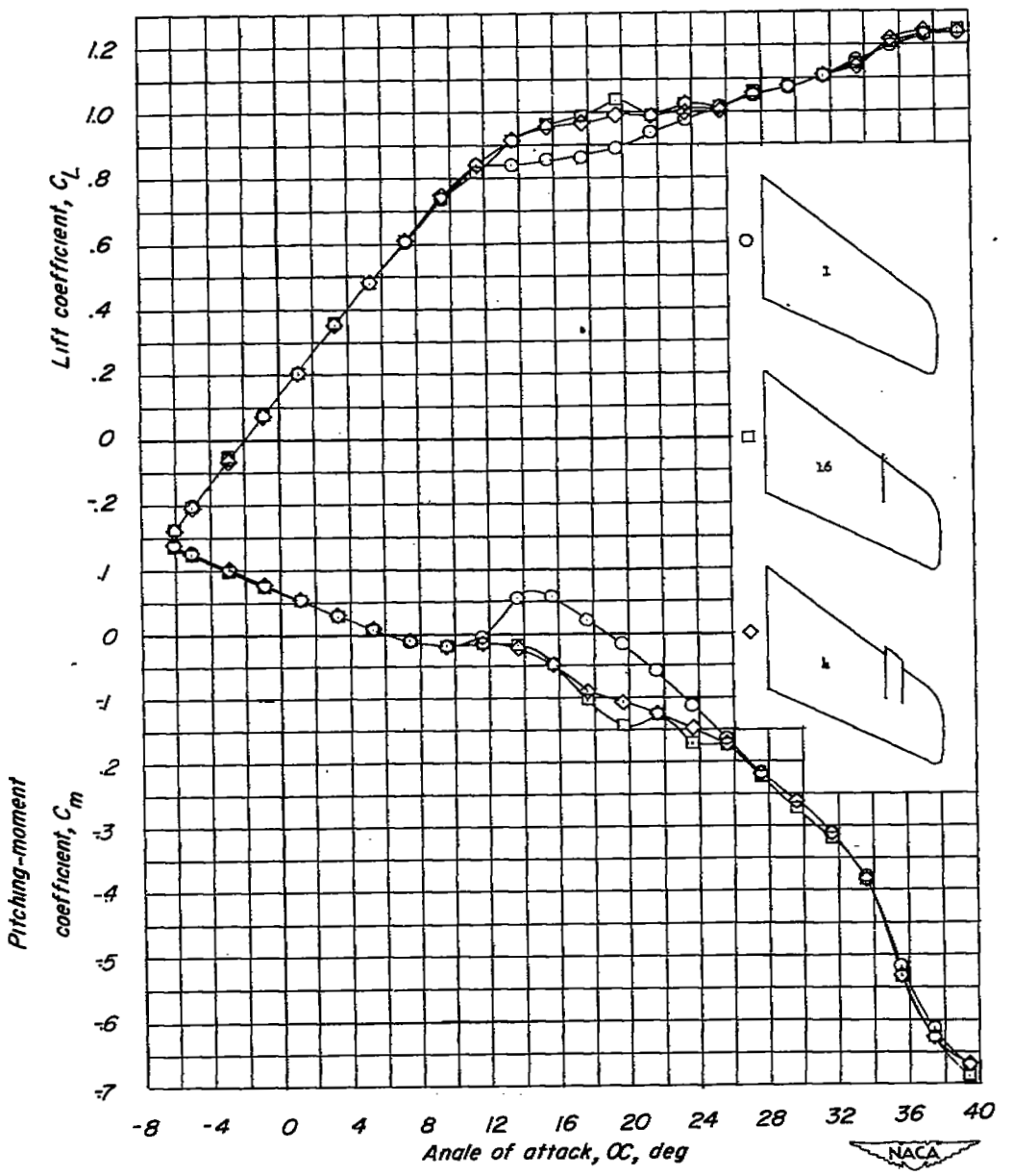

Figure 9.- Comparison of longitudinal stability characteristics of several model configurations. W + F + V + H.

[redacted]

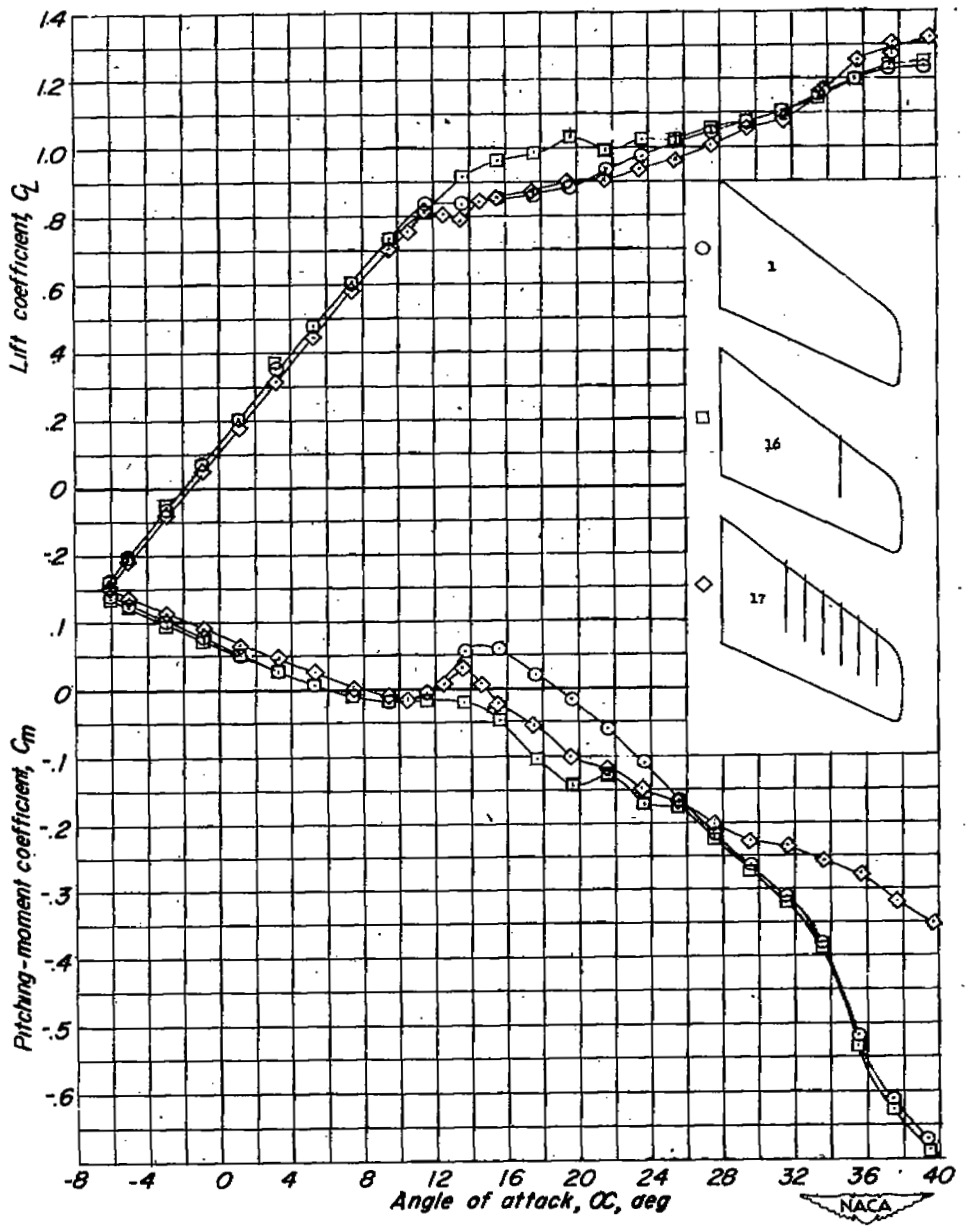

Figure 10.- Comparison of longitudinal stability characteristics of several model configurations. W + F + V + H.

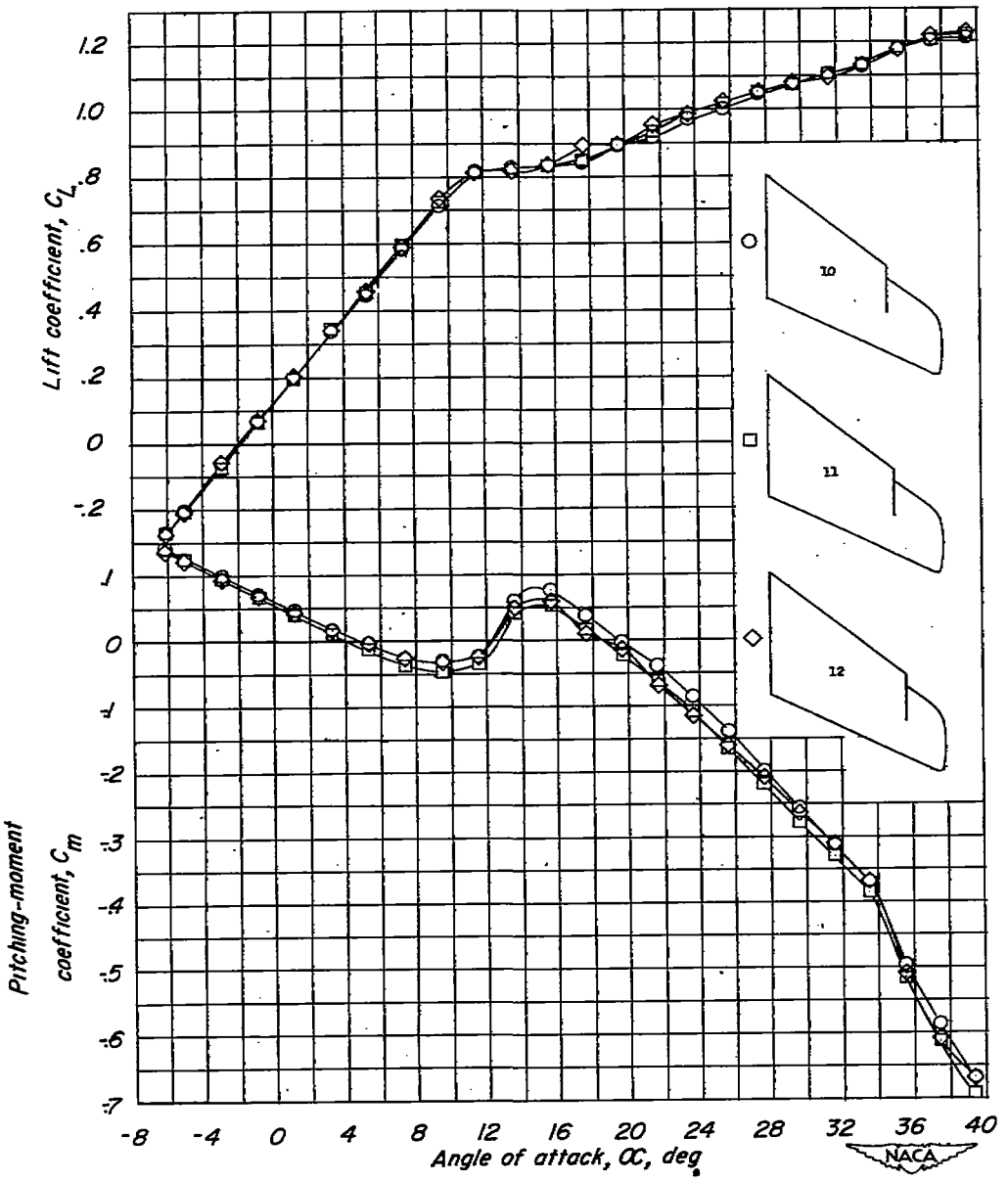

Figure 11.- Comparison of longitudinal stability characteristics of several model configurations. W + F + V + H.

[redacted]

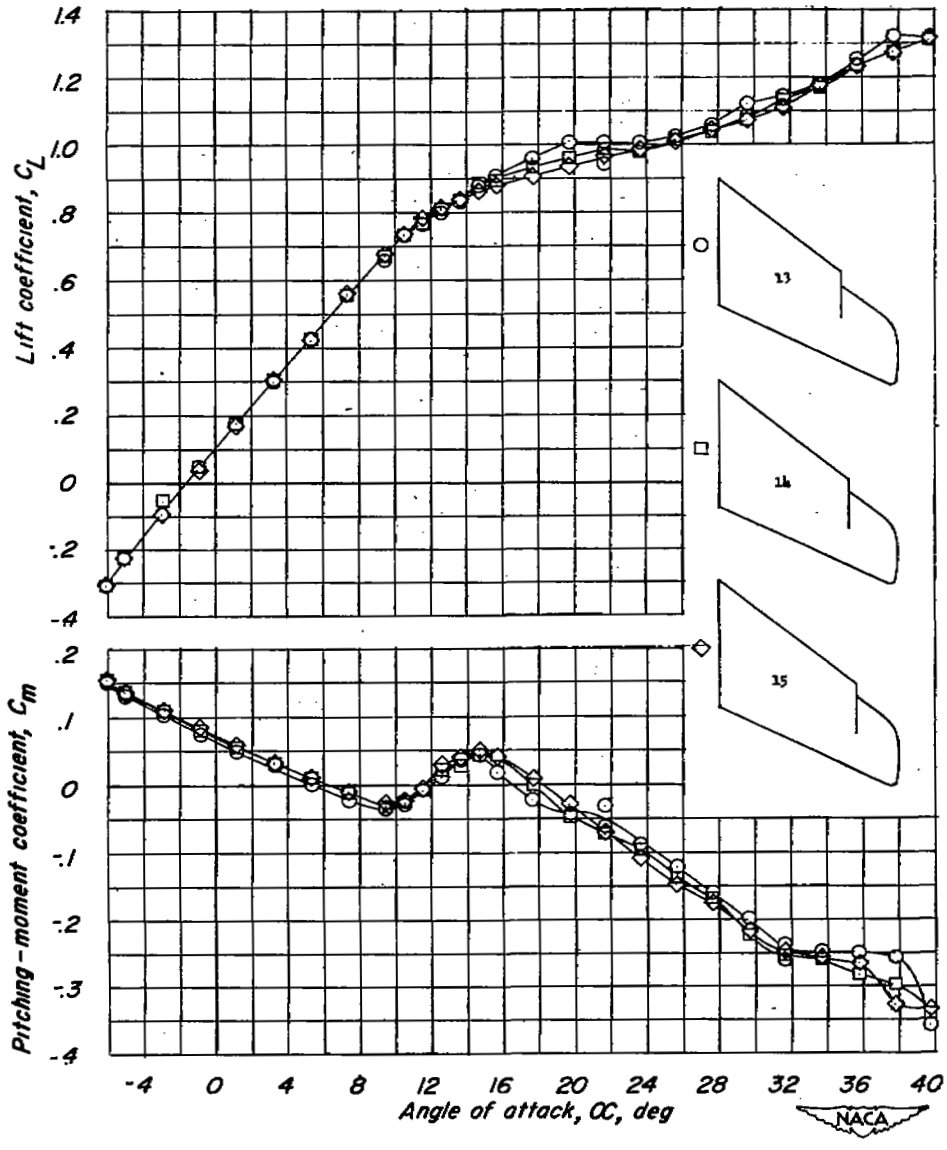

Figure 12.- Comparison of longitudinal stability characteristics of several model configurations. W + F + V + H.

[redacted]

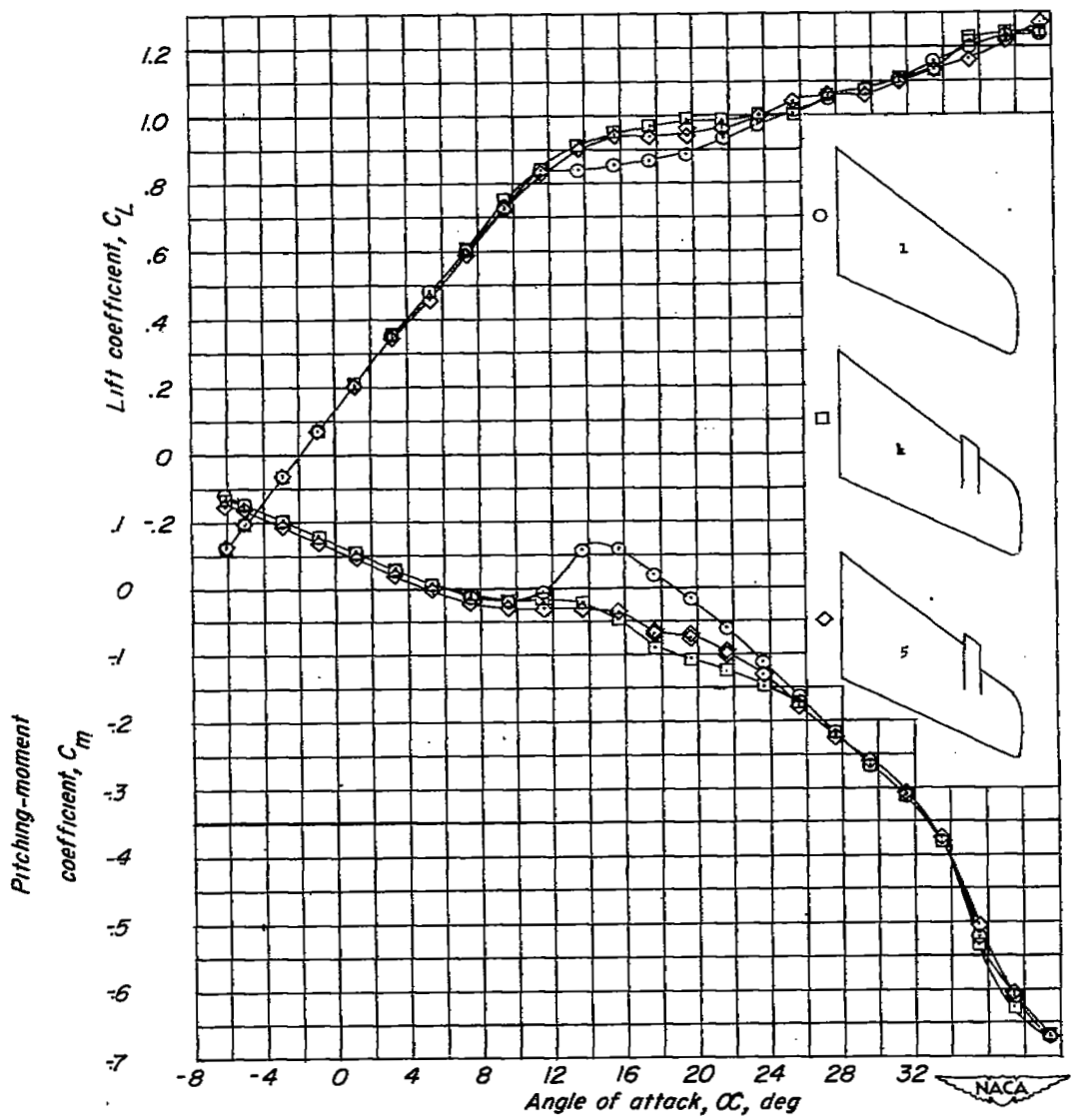

Figure 13.- Comparison of longitudinal stability characteristics of several model configurations. W + F + V + H.

[redacted]

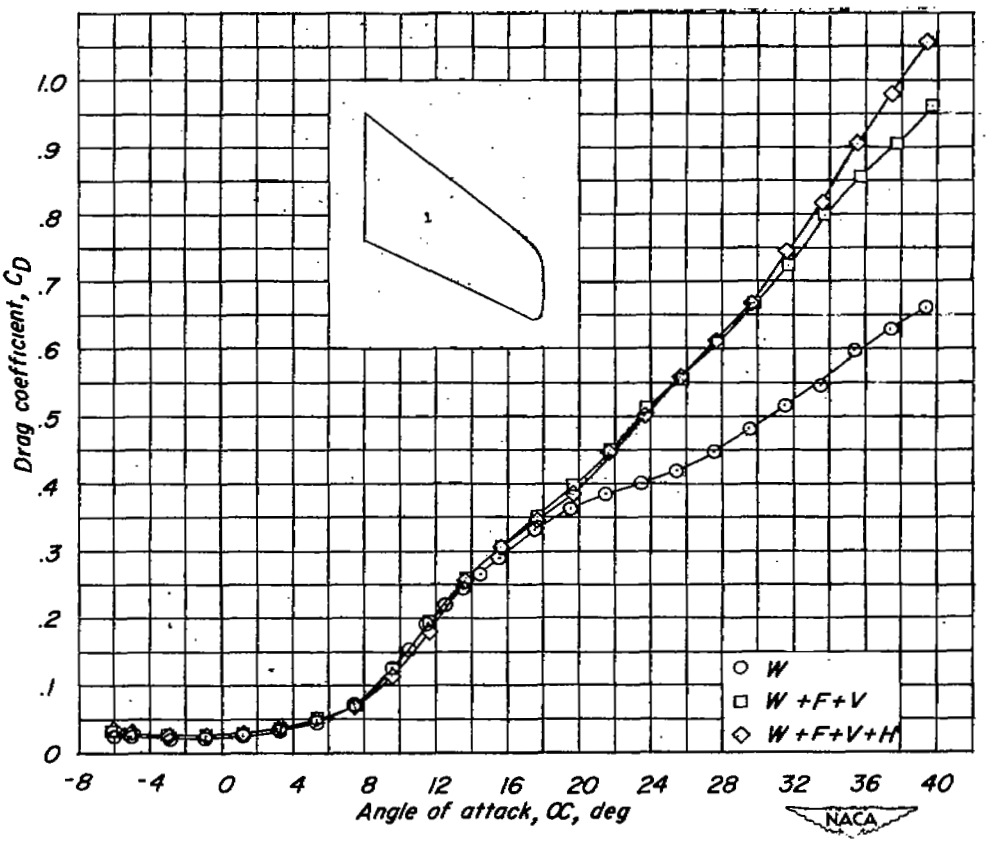

Figure 14.- Drag characteristics of an airplane model having a 35° sweptback wing.

[redacted]

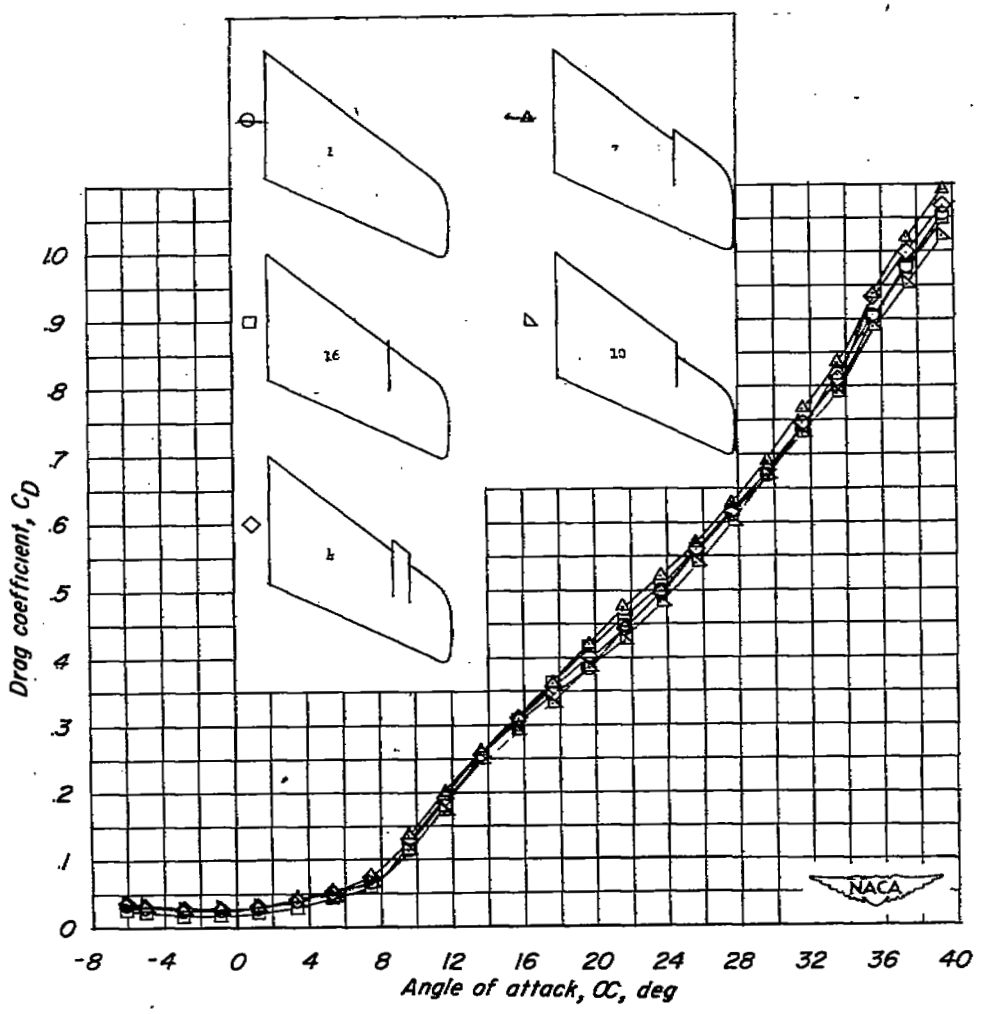

Figure 15.- Comparison of drag characteristics of several model configurations. W + F + V + H.

[redacted]

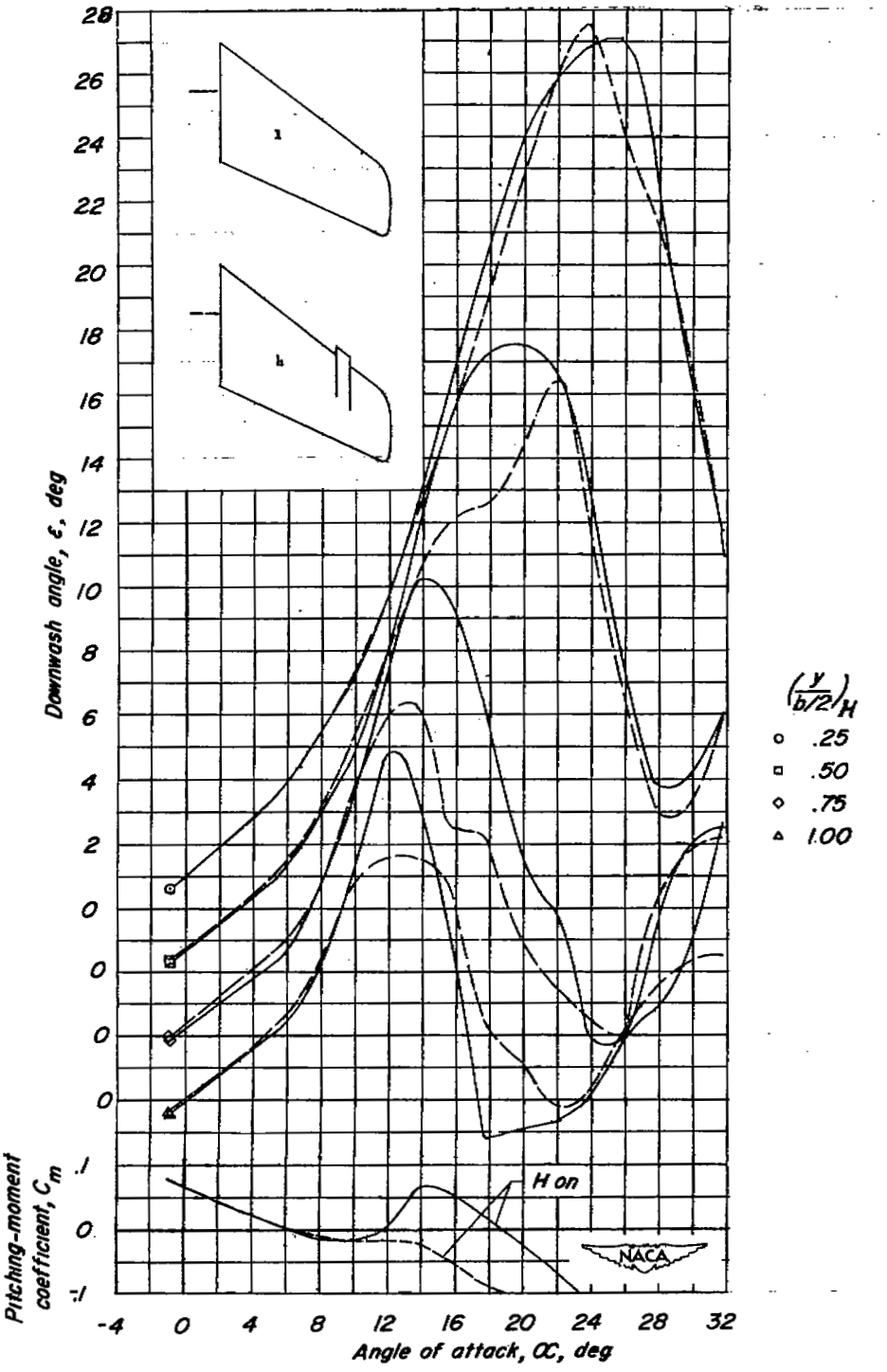

(a) ϵ and C_m against α.

Figure 16.- Comparison of the wake characteristics of several model configurations. W + F + V.

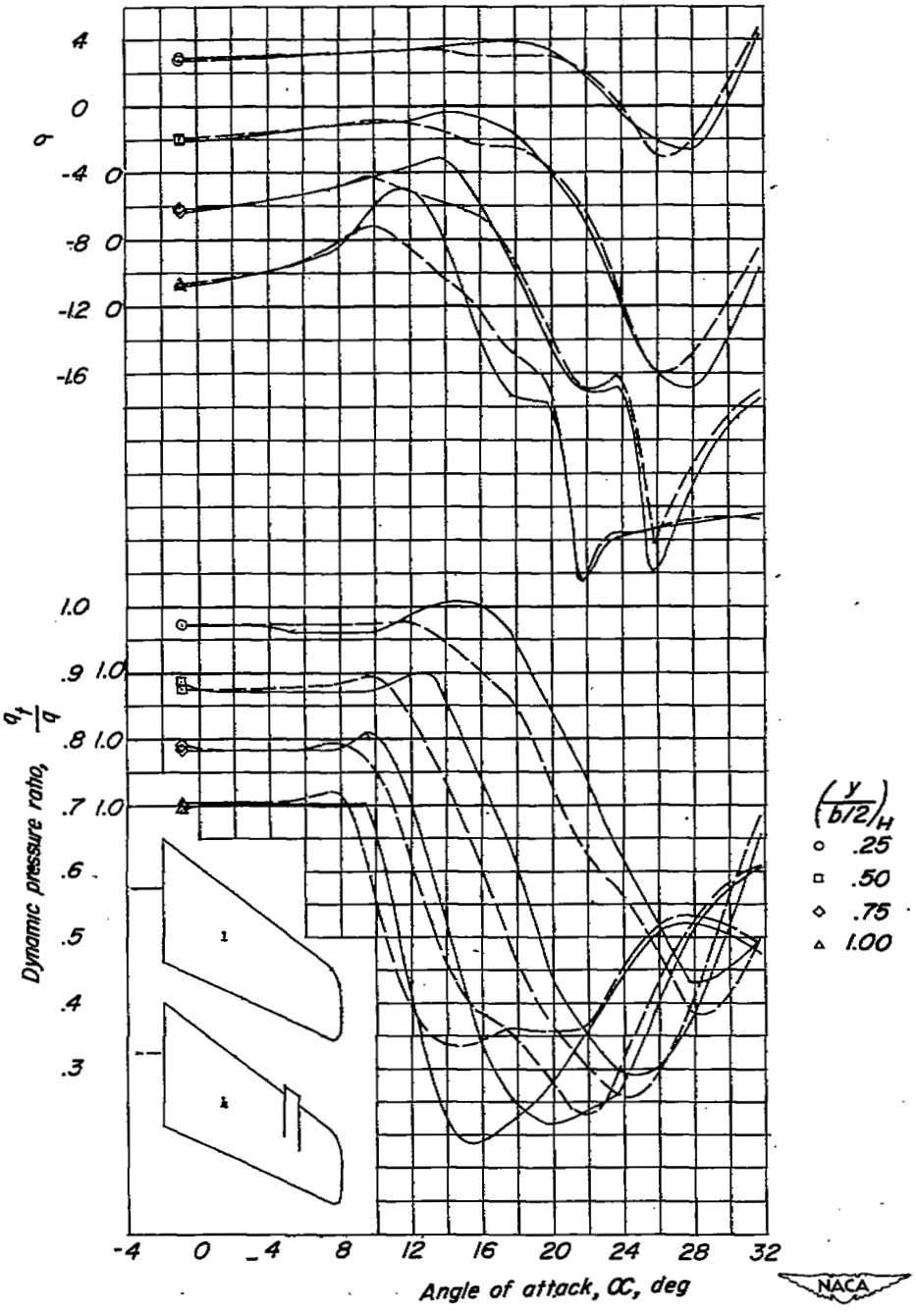

(b) σ and q_t/q against α.

Figure 16.- Concluded.

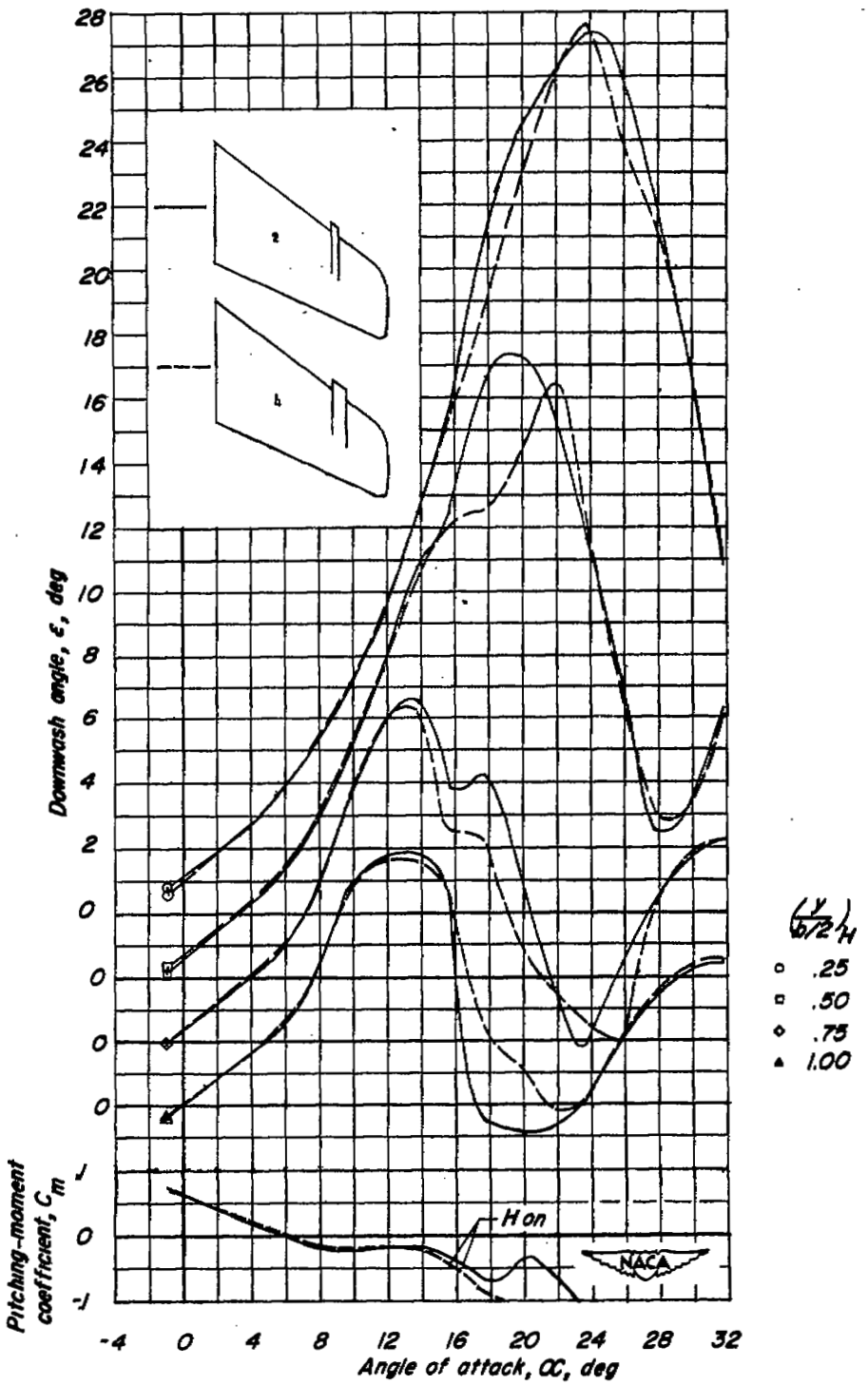

(a) ϵ and C_m against α.

Figure 17.- Comparison of the wake characteristics of several model configurations. W + F + V.

[redacted]

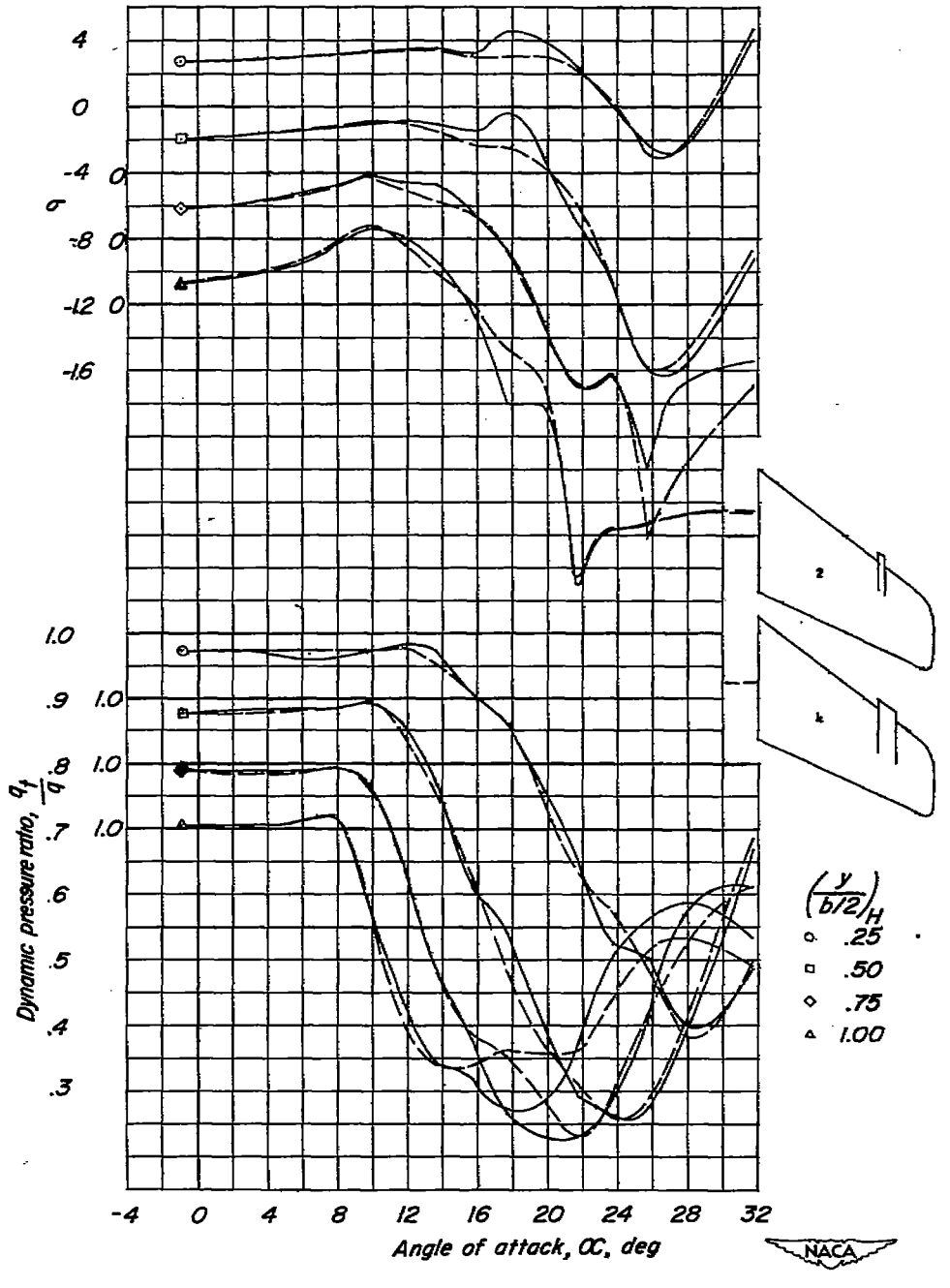

(b) σ and q_t/q against α.

Figure 17.- Concluded.

[redacted]

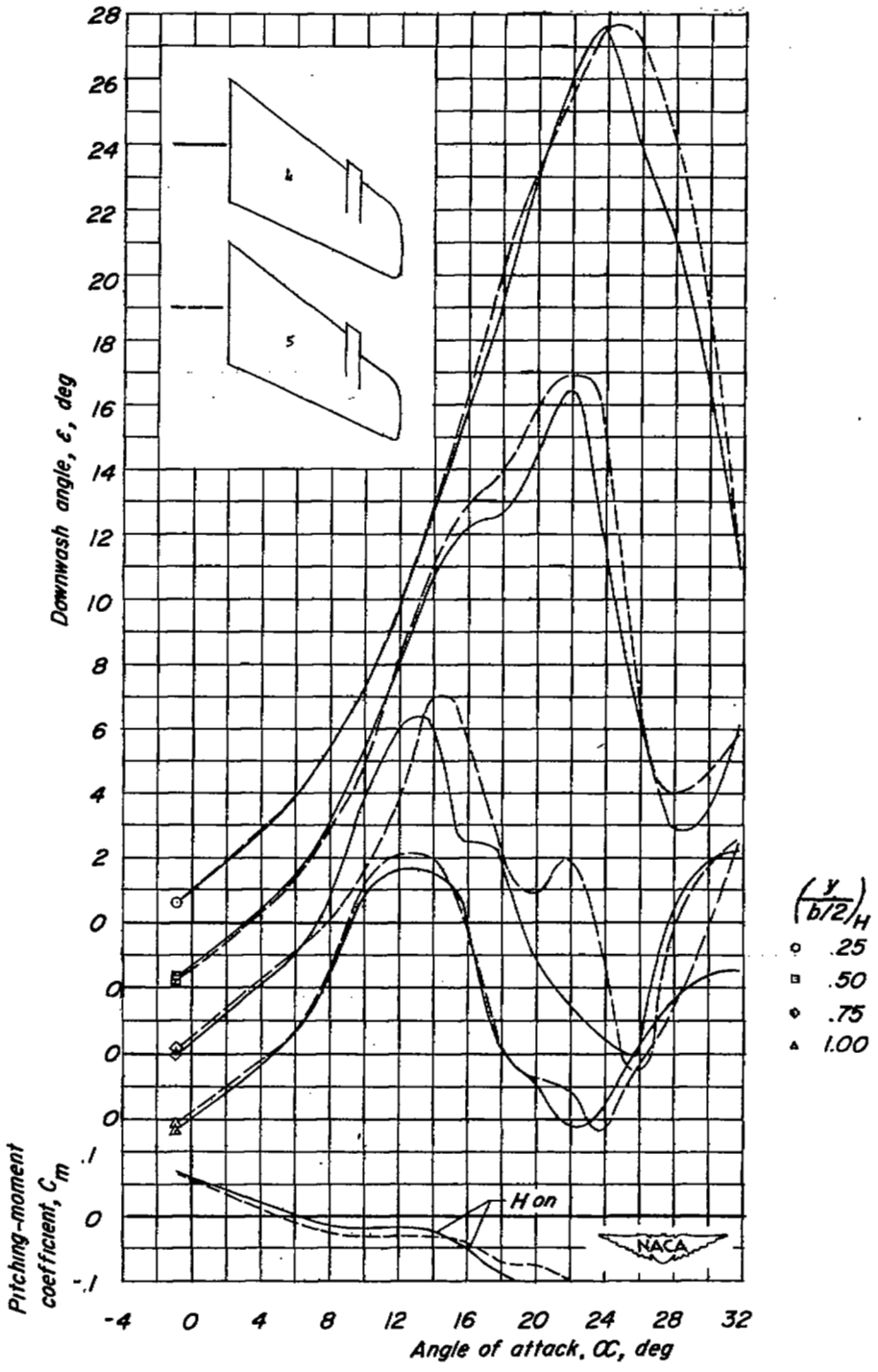

(a) ϵ and C_m against α.

Figure 18.- Comparison of the wake characteristics of several model configurations. W + F + V.

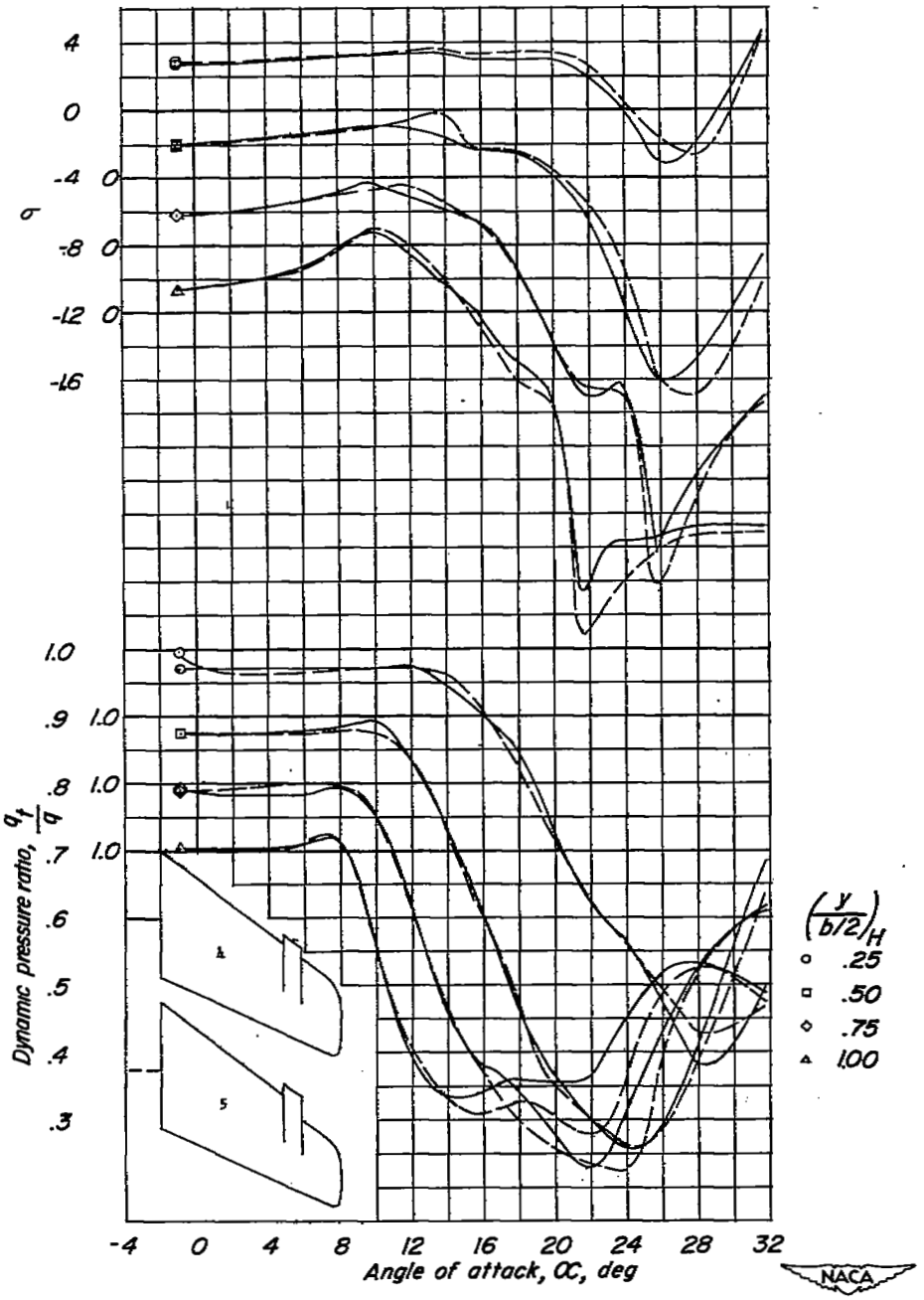

(b) σ and q/q_t against α.

Figure 18.- Concluded.

[redacted]

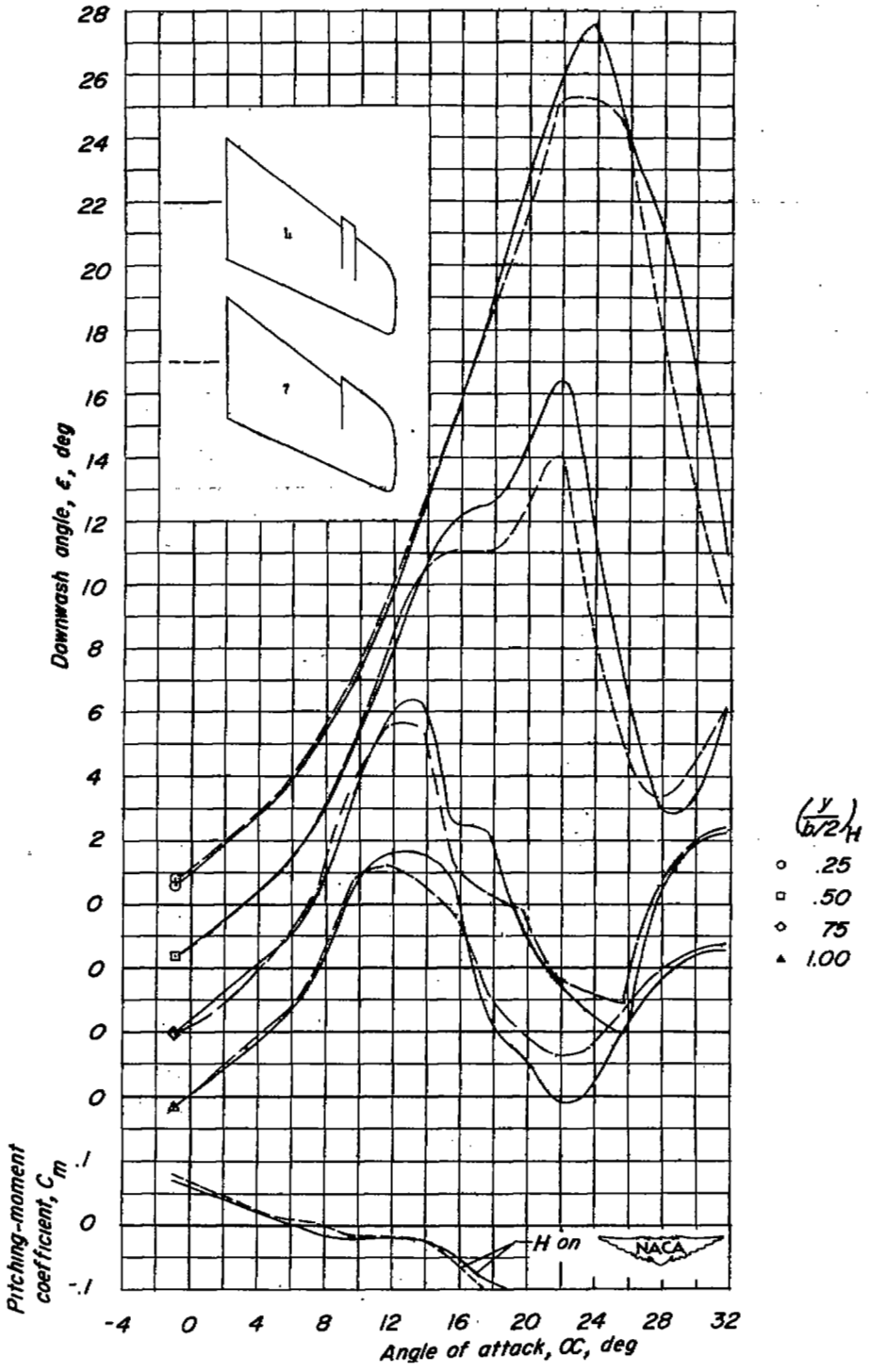

(a) ϵ and C_m against α.

Figure 19.- Comparison of the wake characteristics of several model configurations. W + F + V.

[redacted]

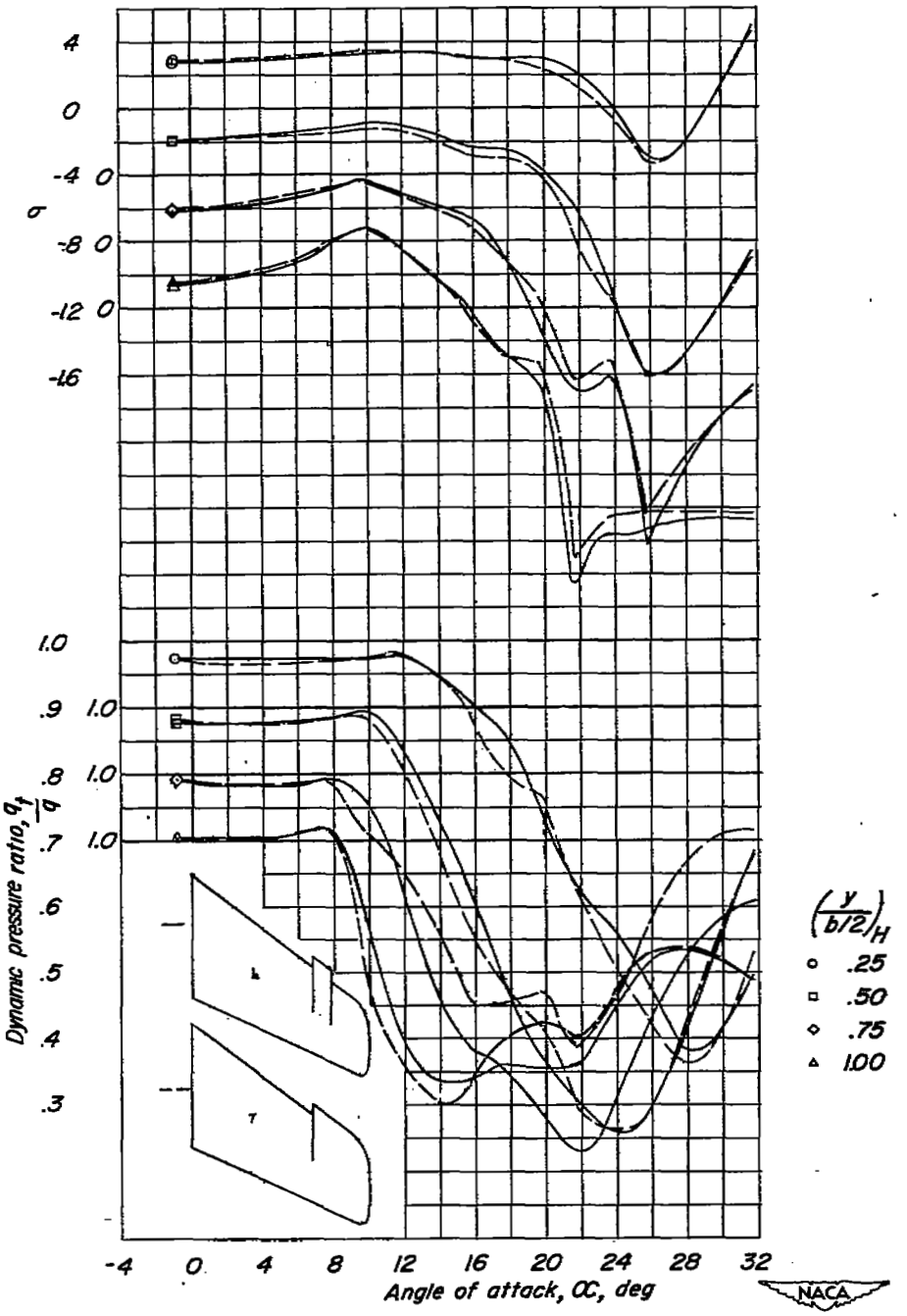

(b) σ and q_t/q against α.

Figure 19.- Concluded.

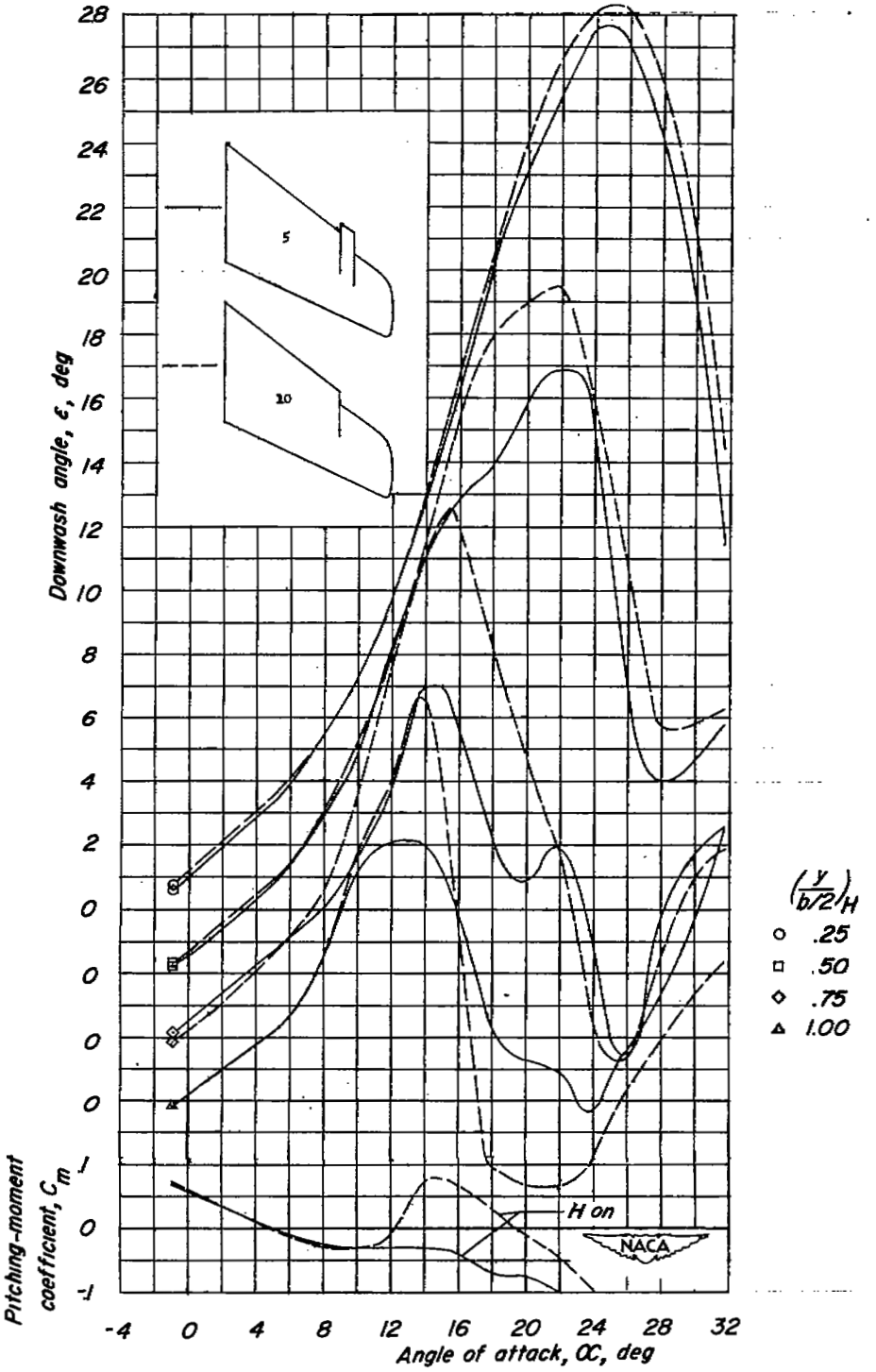

(a) ϵ and C_m against α.

Figure 20.- Comparison of the wake characteristics of several model configurations. W + F + V.

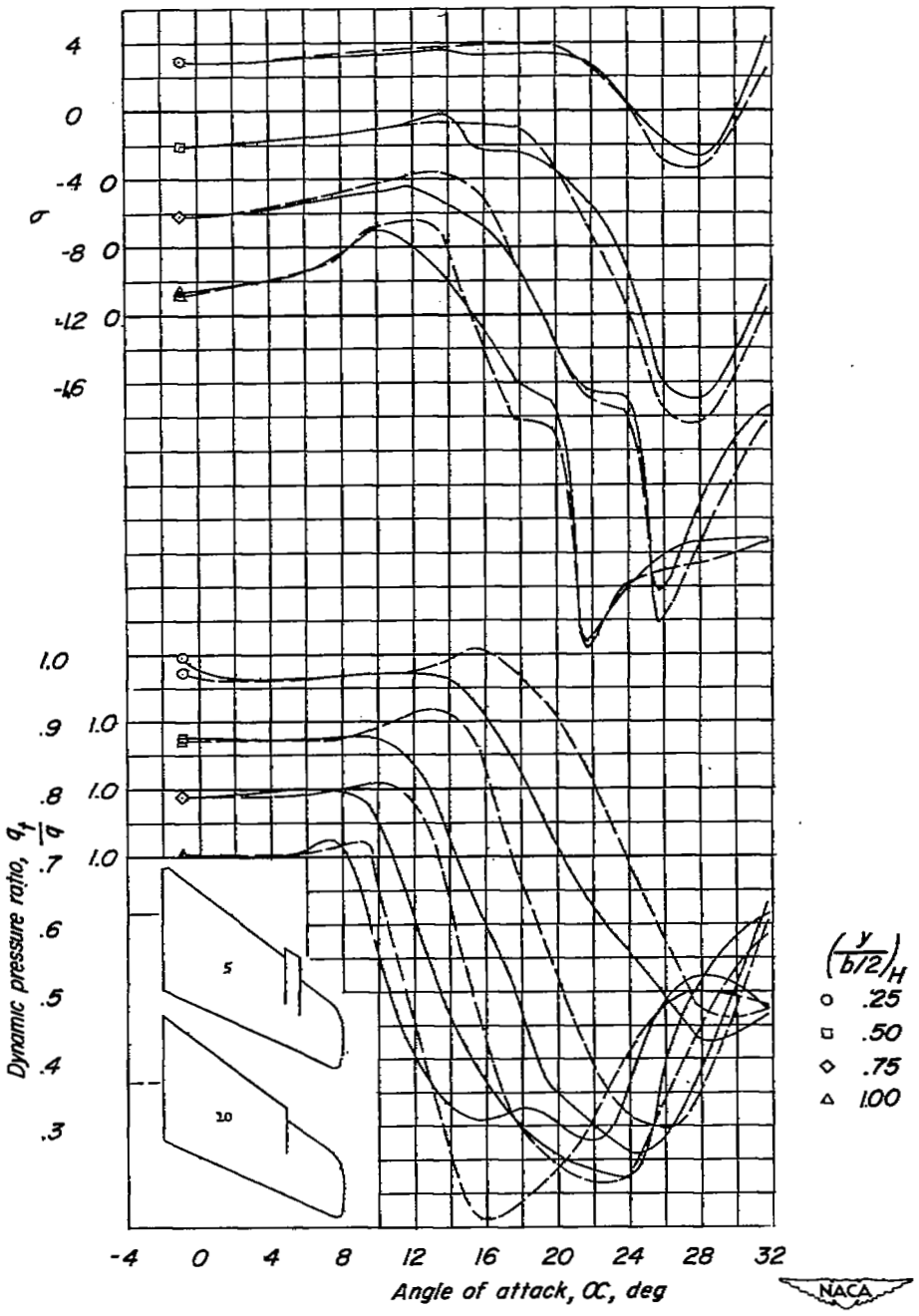

(b) σ and q_t/q against α.

Figure 20.- Concluded.

[redacted]

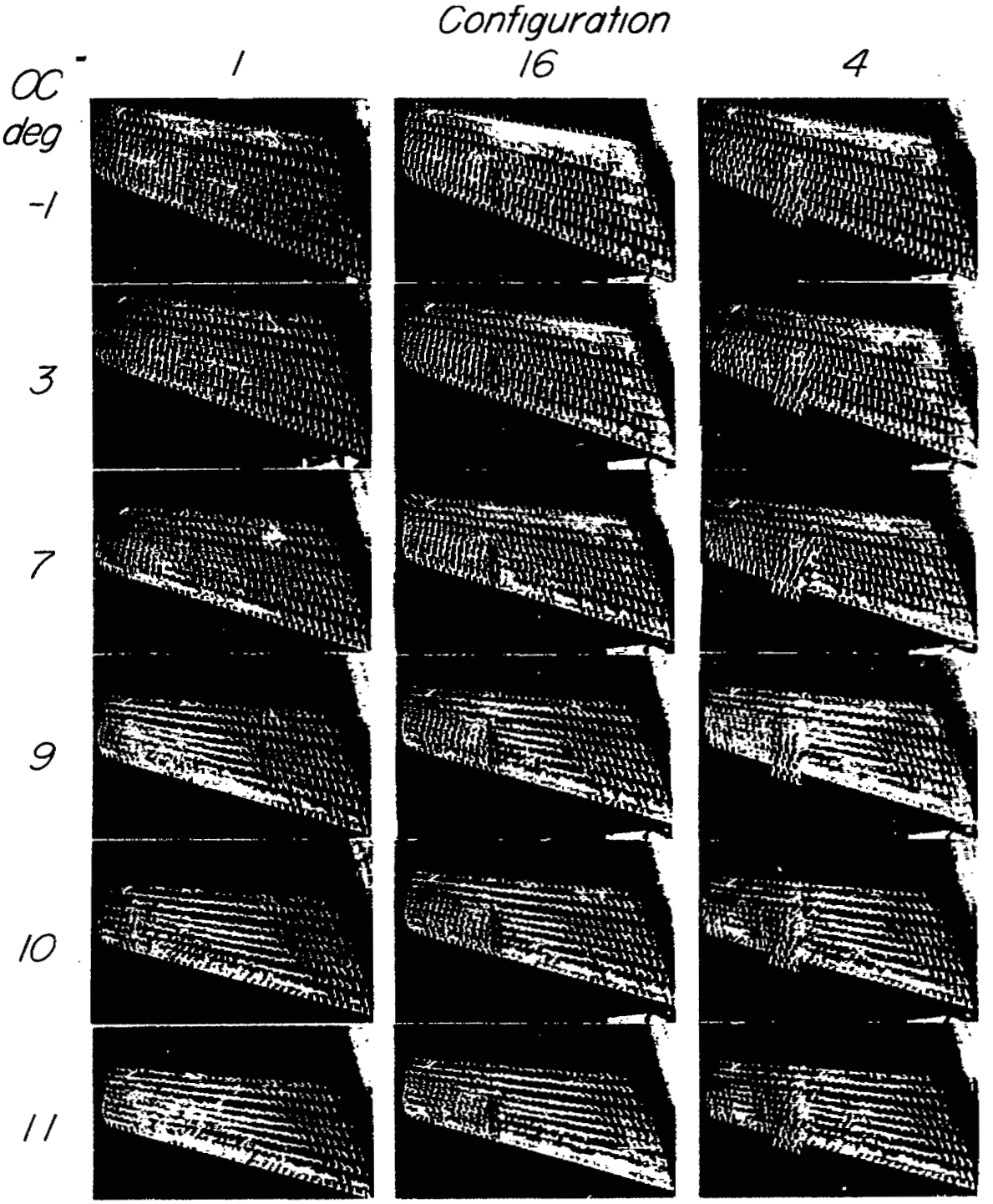

Figure 21.- Surface-tuft photographs ($R = 0.885 \times 10^6$) for several model configurations and tuft-grid photographs ($R = 0.493 \times 10^6$) for configuration 1.

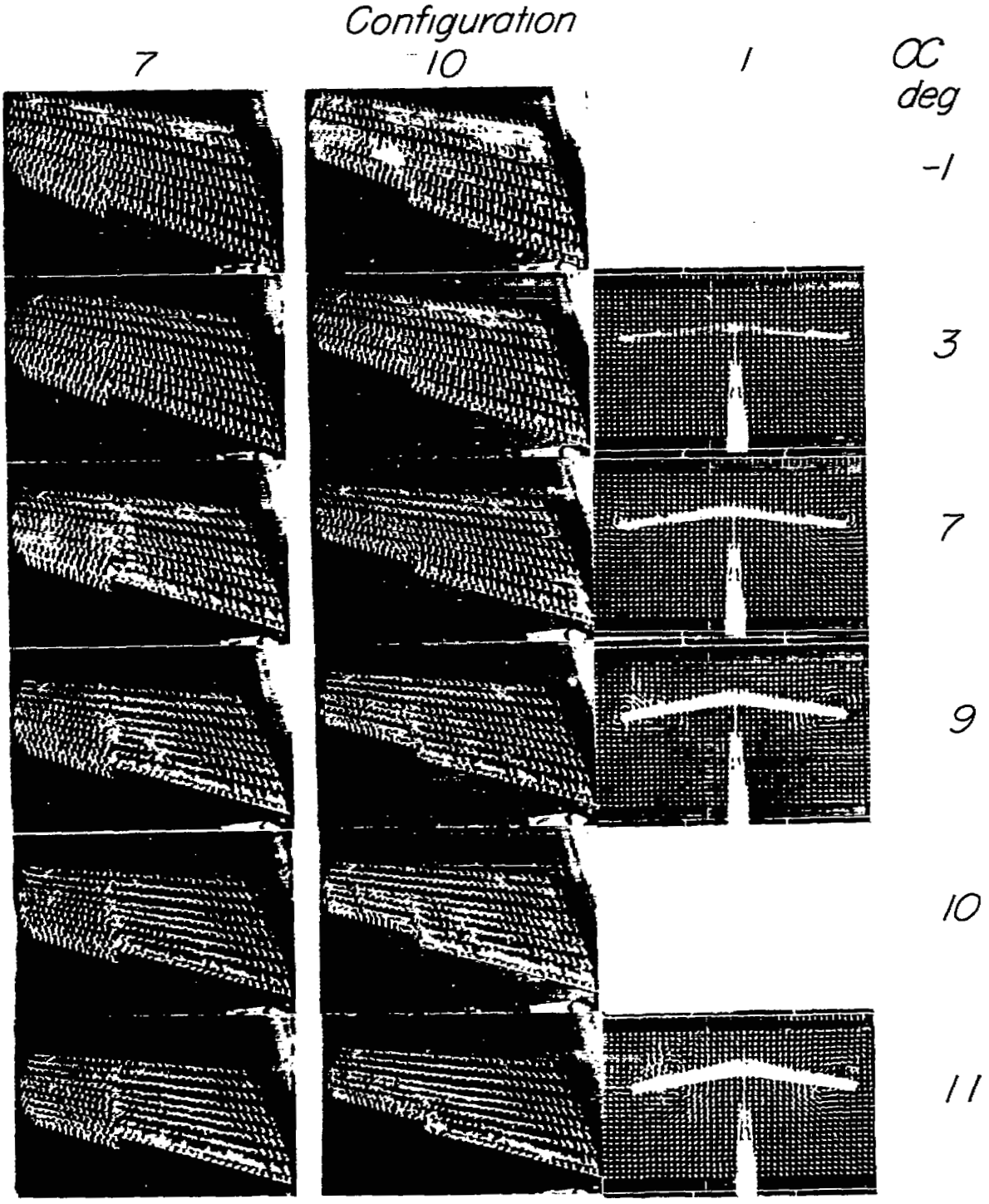

Figure 21.- Continued.

NACA
L-74356

[redacted]

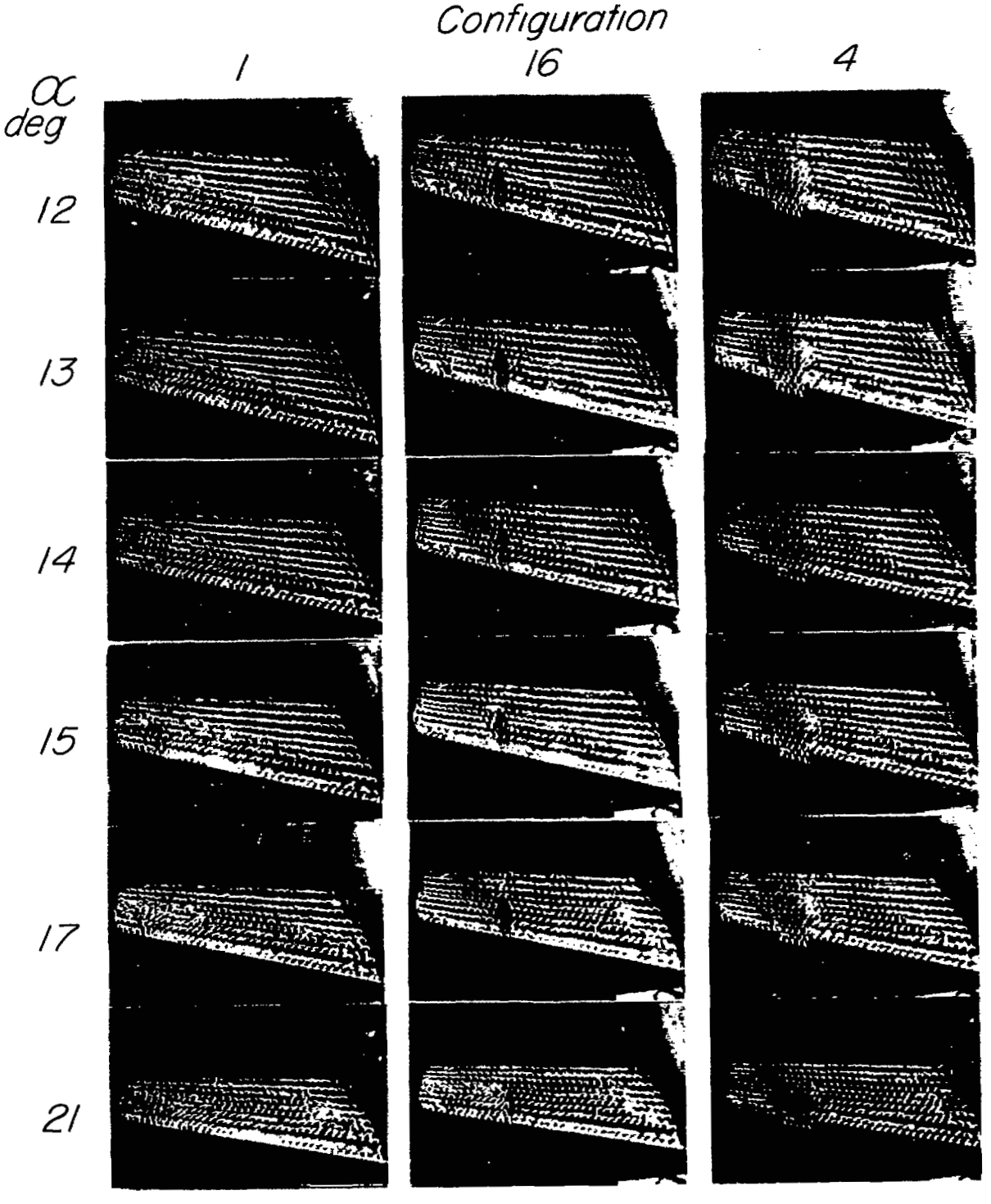

Figure 21.- Continued.

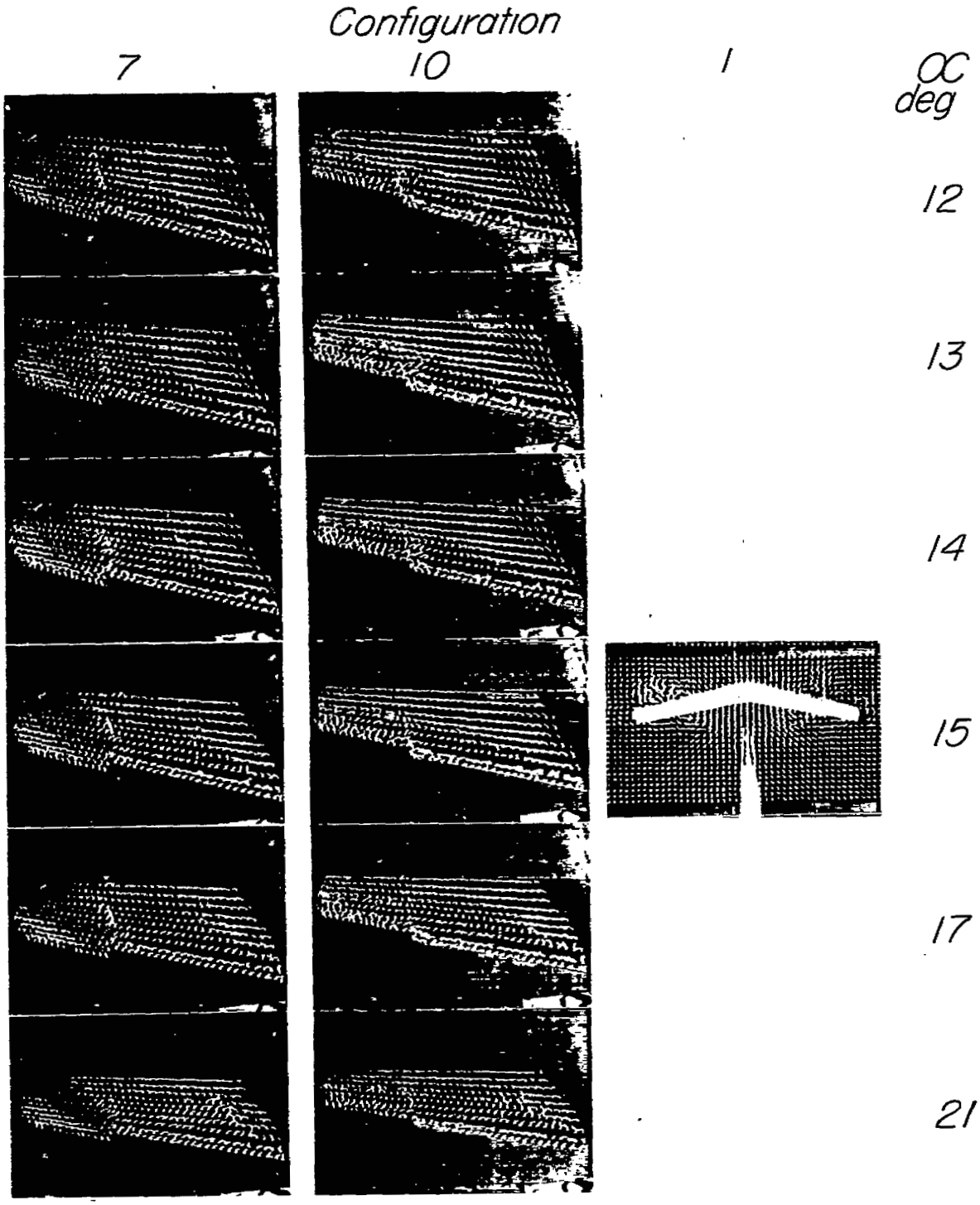

Figure 21.- Concluded.

NACA
L-74357

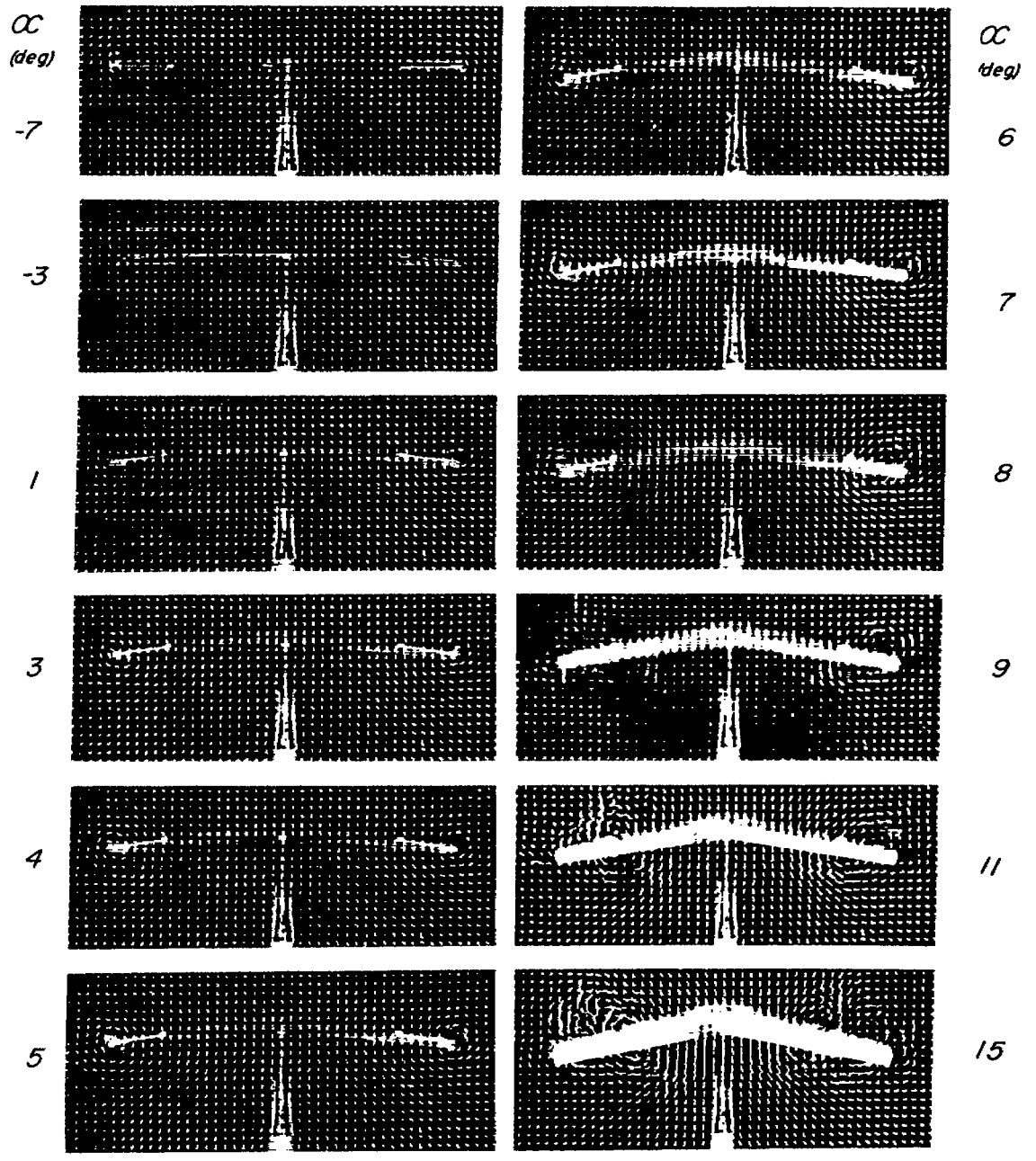

NACA
L-74358

Figure 22.- Tuft-grid photographs of configuration 1. $R = 0.493 \times 10^6$.

NACA-Langley - 6-24-52 -325

[redacted]

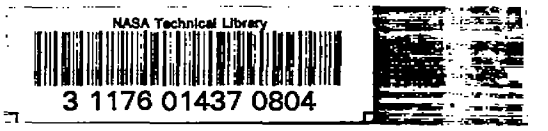

[redacted]